FOUNTAIN JOURNAL OF NATURAL & APPLIED SCIENCES

A Publication of the College of Natural & Applied Sciences
Fountain University, Osogbo, Nigeria

Hydrocarbon source-rock potential of Maastrichtian Araromi shales from a well in the eastern Dahomey basin, southwestern Nigeria: Evidence from TOC and rock-eval pyrolysis

Tukur, M.A., Adekeye, O. A.

Department of Geology and Mineral Sciences, University of Ilorin, Ilorin, Nigeria

*Corresponding author: abdulkadirtukur99@gmail.com

ABSTRACT

The Dahomey Basin is hydrocarbon-bearing but less explored than the neighbouring Niger Delta. This study evaluated the organic geochemistry of 20 Maastrichtian shale samples from the Araromi Formation in a well (1128–2181 m) in southwestern Nigeria. Samples were analysed by Rock-Eval pyrolysis and TOC to assess organic richness, kerogen type, thermal maturity and hydrocarbon potential across the Lower (n = 4), Middle (n = 11) and Upper (n = 5) Maastrichtian. Mean TOC was highest in the Lower Maastrichtian (3.12 wt%), followed by the Upper (2.18 wt%) and Middle (1.39 wt%). Hydrogen index values (195.51–601.03 mg HC/g TOC) indicate mainly Type II and Type II/III kerogen, with mixed oil- and gas-prone potential. The Lower interval had the greatest generative potential (mean S1+S2 of 12.37 mg HC/g rock, versus 6.74 for the Upper and 6.33 for the Middle). Maturity indicators (Tmax 427–612ºC; apparent %Ro 0.53–3.86) varied widely, with the highest means in the Lower interval. Statistical analyses (ANOVA, PCA, HCA, K-Means) showed significant vertical heterogeneity, and the Lower interval differed significantly from both younger intervals. PC1 (53.7%) reflected organic richness and PC2 (21.4%) thermal maturity. Lower Maastrichtian samples clustered together and showed better source-rock quality. The findings are relevant to petroleum-system modelling, and further study of deeper Lower Maastrichtian horizons is recommended.

ARTICLE INFO

Article history:
Received September 2026
Revised October 2026
Accepted October 2026

Keywords:
Hydrocarbon, Geochemistry, Maturation, Kerogen, Pyrolysis

This work is licensed under the Creative Commons Attribution 4.0 International License

Introduction

Today, the world still relies heavily on hydrocarbon resources, and many sedimentary basins have known or suspected petroleum systems of interest. In any petroleum system, the source rock is the most basic component of it, which comprises fine-grained sediment containing a sufficient amount of organic matter to generate and expel commercial hydrocarbons [1, 2]; hence, understanding the organic content, quality and maturity of the source rocks is crucial to evaluate the basin viability [3-5].

The West African Atlantic margin is characterised by sedimentary basins which were developed during the Mesozoic rifting of South America from Africa [6]. The Dahomey (Benin) Basin lies in southeastern Ghana and extends into Togo and Benin, southwest of Nigeria, bordered to the west by the Ghana Ridge and to the east by the Benin Hinge Line, which separates it from the Niger Delta [7, 8]. Although the eastern (Nigerian) Dahomey Basin lies within a prolific hydrocarbon province, it has been explored far less than the adjacent Niger Delta Basin, probably because of its perceived lower potential and challenging structural history [9, 10].

The Dahomey Basin stratigraphic sequence consists of Cretaceous to Recent sediments that reach a maximum thickness of 9 km in the Nigerian part of the basin [11, 12]. The Cretaceous Abeokuta Group is divided into the marine shales of the Araromi Formation in the upper part, the middle Afowo Formation (interbedded sandstones and shales with brackish-marine influence) and the continental sands/grits of the Ise Formation at the base [13, 14]. The fine-grained lithology, organic-richness and lateral continuity of the Araromi Formation are of particular interest in source-rock evaluation, and its

DOI: https://doi.org/10.53704/fujnas.v15i2.1572

foraminiferal and palynological assemblage has been dated as Maastrichtian [15].

Previous studies by Falufosi & Osinowo [6], Adeigbe & Oyekola [13], and Gebhardt et al. [16] established the basin's lithostratigraphic framework and biostratigraphic zonation, while Falufosi & Osinowo [6] established its tectonic evolution. Organic geochemical studies have revealed that the organic matter is predominantly gas-prone in the Maastrichtian-Eocene sediments [17]; studies have been conducted on the hydrocarbon potential of the Upper Cretaceous-Lower Tertiary sediments [18], and the principal source rocks have been identified, where the shallow Araromi shales are often immature to marginally mature [17, 18]. Recent studies show that organic matter in shallow Araromi and Gbekebo wells is mostly reworked Type III, while deeper wells and mature Cenomanian offshore rocks may contain oil-prone Type II marine kerogen [17, 18].

Despite these contributions, key gaps remain. Although many studies have been performed on the Araromi Formation, very few have addressed the possibility of vertical variation in source-rock character across the Maastrichtian, which could possibly result in stratigraphic variations in richness, kerogen type and maturity. The burial depth–generation potential relationship in the Nigerian sector remains poorly constrained, particularly at depths where the reservoir is more thermally mature. The Maastrichtian interval, although lithologically and organically favourable, is relatively under-studied, although sequences related to the older Oceanic Anoxic Event 2 have been studied regionally [10].

This study aims to fill these gaps by conducting a detailed organic geochemical characterisation of Maastrichtian shales subdivided into Lower, Middle, and Upper depth-defined intervals and correlated with previous regional stratigraphic studies [19]. In a well that penetrates the Araromi Formation in the eastern Dahomey Basin. The aim is to: (1) determine the organic richness and generation potential using TOC and Rock-Eval pyrolysis data; (2) determine the kerogen types and the implications for oil versus gas generation; (3) assess thermal maturity using the Tmax and Tmax-derived apparent vitrinite reflectance data; and (4) examine the relation between the burial depth and the hydrocarbon-generation potential to determine the best source-rock interval within the well. The results help clarify the nature of the Maastrichtian source rocks in the eastern Dahomey Basin and provide insight into the overall petroleum system of the Gulf of Guinea, considering similar West African margin basins.

Geological setting

The Dahomey Basin is a marginal basin of the Gulf of Guinea province, extending from the southeast of Ghana to Togo and Benin and to the southwest of Nigeria, with the Ghana Ridge (Romanche Fracture Zone extension) to the west and the Benin Hinge Line to the east, which separates it from the Niger Delta [20, 21]. The basin was formed during the Late Jurassic-Early Cretaceous rifting associated with the separation of South America and Africa, and the development of the basin in Nigeria has been divided into four phases: pre-rift, syn-rift, transitional and post-rift, which resulted in the formation of horst and graben structures and up to 3 km of Cretaceous-Recent sediment accommodation [17, 22].

The Cretaceous Abeokuta Group of the Dahomey Basin consists of the basal Ise Formation (continental sands/grits, Neocomian – Albian), middle Afowo Formation (interbedded sandstones/shales with brackish-marine influence, Turonian) and the upper Araromi Formation (marine shales with thin limestone and lignite interbeds, Maastrichtian), which is the focus of this study; Mohammed et al. [23] and Alege et al. [24]. The richly fossiliferous Araromi Formation (with abundant plankton and benthic foraminifera, ostracods and palynomorphs [22, 24, 25] is followed by the shallow marine limestone Ewekoro Formation and the succeeding Eocene Oshosun and Ilaro Formations [7, 26]. Past geochemical work suggests the Cenomanian–Turonian sequences as the key source rocks containing Type II marine kerogen, and the Maastrichtian Araromi shales as mostly gas-prone, with Type III kerogen at shallow depths but Type II at deeper levels, which may be mature enough to generate liquid hydrocarbons [18, 22, 27].

Materials and methods

Sample collection

Drill core samples were taken from Well X, located in the eastern Dahomey Basin, southwestern Nigeria (~6°30'N, 4°00'E). The well intersected the Araromi Formation between 1128 and 2181 m, with core recovery over 85%. Samples from an indigenous oil company consist mainly of grey and dark-grey shales, some sandy shales and occasional glauconitic horizons.

There were twenty (20) representative shale samples that were selected based on lithological variation and stratigraphic distribution: five (5) Upper

DOI: https://doi.org/10.53704/fujnas.v15i2.1572

Maastrichtian (1128-1254 m), eleven (11) Middle Maastrichtian (1287-1980 m) and four (4) Lower Maastrichtian (2028-2181 m) samples using depth-defined intervals (although not independently dated) correlated to the regional stratigraphic frameworks of Omatsola & Adegoke [28] and Adekeye [29]. Samples, depths and lithology are provided in Table 1.

Table 1: ***Summary of sample depths, lithology, and stratigraphic intervals.***

Interval	Sample ID	Depth (m)	Lithology
Upper Maastrichtian	WX-01	1128	Black shale
Upper Maastrichtian	WX-02	1158	Black shale
Upper Maastrichtian	WX-03	1191	Shale
Upper Maastrichtian	WX-04	1224	Shale
Upper Maastrichtian	WX-05	1254	Black shale
Middle Maastrichtian	WX-06	1287	Shale
Middle Maastrichtian	WX-07	1323	Shale
Middle Maastrichtian	WX-08	1353	Shale
Middle Maastrichtian	WX-09	1389	Shale
Middle Maastrichtian	WX-10	1419	Shale
Middle Maastrichtian	WX-11	1578	Grey shale
Middle Maastrichtian	WX-12	1608	Grey shale
Middle Maastrichtian	WX-13	1665	Grey shale
Middle Maastrichtian	WX-14	1695	Shale
Middle Maastrichtian	WX-15	1728	Shale
Middle Maastrichtian	WX-16	1980	Shale
Lower Maastrichtian	WX-17	2028	Black shale
Lower Maastrichtian	WX-18	2100	Black shale
Lower Maastrichtian	WX-19	2133	Black shale
Lower Maastrichtian	WX-20	2181	Black shale

Organic geochemistry

All analyses were done at Weatherford Laboratories, USA, using standard procedures, with samples being ground to <200 mesh before analysis.

TOC was measured using a LECO CS-230 carbon-sulfur analyser: ~100 mg of pulverised sample was treated with HCl to remove carbonates, combusted in oxygen, and the evolved CO_2 was measured by infrared detection (wt%). Quality control included certified reference materials and replicate analyses of every fifth sample, yielding a precision of < ±5% RSD.

The Rock-Eval pyrolysis was performed according to Espitalié et al. [30] with a Rock-Eval 6 pyrolyser, where ~100 mg of the samples were heated at 300°C for 3-4 minutes under helium to liberate free hydrocarbons (S1) and pyrolysed at 25°C/min from 300-600°C to crack kerogen and generate pyrolytic hydrocarbons (S2), with CO_2 (S3) measured by thermal conductivity detection and Tmax obtained at the maximum S2. The IFP 160000 standard was used for the daily calibration, and replicate analyses were made to assess reproducibility, with S1 > 1 mg HC/g rock considered indicative of possibly migrated hydrocarbons.

Derived parameters: Hydrogen Index HI = (S2/TOC)×100 (mg HC/g TOC); Oxygen Index OI = (S3/TOC)×100 (mg CO_2/g TOC); Production Index PI = S1/(S1+S2); Petroleum Potential = S1+S2 (mg HC/g rock); Tmax-derived apparent vitrinite reflectance %Ro = (0.0180×Tmax) – 7.16 [31].

Kerogen types were interpreted from HI–OI (Van Krevelen), HI–Tmax and S2–TOC cross plots after Peters and Cassa [5]. Thermal maturity was determined using Tmax, PI and Tmax-derived %Ro [4, 5]. It is emphasised that these %Ro values are apparent, Tmax-derived estimates and are not measured vitrinite reflectance. The Jarvie et al. [31] equation is calibrated for Type II/III shales and is unreliable above approximately 1.5–2.0%Ro. Four samples showed unusually high Tmax values (>600°C): WX-04 (607°C), WX-05 (612°C), WX-08 (612°C), and WX-18 (605°C). Repeat analyses were consistent, suggesting that these values are not necessarily analytical artefacts; however, they may reflect local thermal anomalies, reworked or oxidised organic matter, or mineral-matrix effects. Consequently, Tmax-derived apparent %Ro values associated with these anomalously high Tmax values are treated cautiously and should not be regarded as precise maturity measurements.

Statistical analysis

Multivariate analyses were performed using Python 3.10 with scikit-learn (v1.6.1), scipy (v1.16.3), pandas (v2.2.3), pingouin (v0.6.1), matplotlib (v3.10.0), and seaborn (v0.13.2), with variables scaled to zero mean and unit variance. PCA was conducted on TOC, S1, S2, S3, HI, OI, Tmax, PI and apparent_Ro (excluding secondary variables S1+S2 and S2/S3 to prevent redundancy) using biplots (colour-coded by stratigraphic interval; [32, 33]) and retaining components based on the Kaiser criterion and scree-plot inspection. Ward's minimum-variance linkage [34] (on squared Euclidean distances) was applied, with the number of clusters selected by the Elbow method and dendrogram inspection, and cophenetic correlation was used to assess robustness. Differences among the three depth-defined Maastrichtian intervals were evaluated using one-way ANOVA ($p < 0.05$), with Tukey HSD used for pairwise comparisons where appropriate [35] to identify pairs of means that differed, and Levene's test was employed to test the homogeneity of variance and was

DOI: https://doi.org/10.53704/fujnas.v15i2.1572

replaced by Welch's ANOVA/games-howell when the variance was not homogeneous. We quantified linear relationships with Pearson correlations and plotted them as a heatmap with significance annotations; near-perfect correlations were noted due to mathematical derivation (e.g., Tmax and apparent Ro), not independent validation. Linear regression was used to evaluate relationships between depth and maturity parameters, depth and S1+S2, and TOC and S2; R^2 values and 95% confidence intervals were reported.

Results

Organic geochemistry

Table 2 presents the complete Rock-Eval and TOC dataset for the twenty Araromi Formation samples (1128–2181 m; Upper n=5, middle n=11, Lower n=4), revealing substantial stratigraphic variability in organic richness, kerogen quality, and thermal maturity.

Total organic carbon (TOC)

TOC shows a clear stratigraphic trend (Table 2; Fig. 1). Upper Maastrichtian shales range 1.79–2.96 wt% (mean 2.18 ± 0.47 wt%; 25% of samples), classified as good to very good [5]. Middle Maastrichtian samples are more variable, 0.74–1.98 wt% (mean 1.39 ± 0.38 wt%; 55% of samples), with ~27% falling below the 1.0 wt% fair-quality threshold. Lower Maastrichtian shales are significantly richer, 2.24–3.82 wt% (mean 3.12 ± 0.66 wt%; 20% of samples), consistently very good, with the maximum (3.82 wt%) at 2100 m. The intra-Middle Maastrichtian variability likely reflects changing depositional conditions or organic input; overall, the Lower Maastrichtian shales possess the best TOC values.

Table 2: ***Rock–Eval pyrolysis data for the Araromi formation.***

Age	Depth (m)	TOC (wt%)	S1	S2	S3	S2/S3	Tmax (°C)	Tmax-derived. %Ro	HI	OI	PI	S1+S2
Upper	1128	2.96	1.54	5.86	1.01	5.80	449	0.91	197.97	34.12	0.21	7.40
Upper	1158	2.31	1.44	4.97	0.75	6.63	445	0.84	215.15	32.47	0.22	6.41
Upper	1191	1.79	1.57	4.40	0.73	6.03	447	0.89	245.81	40.78	0.26	5.97
Upper	1224	1.84	1.70	5.06	0.67	7.55	607	3.77	275.00	36.41	0.25	6.76
Upper	1254	2.00	1.70	5.45	0.65	8.38	612	3.86	272.50	32.50	0.24	7.15
Mid	1287	1.78	1.23	3.48	0.81	4.30	562	2.96	195.51	45.51	0.26	4.71
Mid	1323	1.98	2.08	6.18	0.83	7.45	457	1.07	312.12	41.92	0.25	8.26
Mid	1353	1.62	2.57	6.25	0.55	11.36	612	3.86	385.80	33.95	0.29	8.82
Mid	1389	1.67	1.45	3.52	0.62	5.68	427	0.53	210.78	37.13	0.29	4.97
Mid	1419	1.73	2.58	4.64	0.44	10.55	509	2.00	268.21	25.43	0.36	7.22
Mid	1578	0.97	2.06	5.83	0.63	9.25	529	2.36	601.03	64.95	0.26	7.89
Mid	1608	0.74	1.53	3.24	0.18	18.00	475	1.40	437.84	24.32	0.32	4.77
Mid	1665	0.96	1.50	4.27	0.41	10.41	539	2.55	444.79	42.71	0.26	5.77
Mid	1695	1.48	1.84	5.08	0.39	13.03	428	0.54	343.24	26.35	0.27	6.92
Mid	1728	1.38	1.09	3.03	0.39	7.77	460	1.11	219.57	28.26	0.26	4.12
Mid	1980	1.02	1.80	4.36	0.41	10.63	579	3.25	427.45	40.20	0.29	6.16
Lower	2028	3.19	4.73	6.70	2.01	3.33	590	3.46	210.03	63.01	0.41	11.43
Lower	2100	3.82	4.38	9.12	2.46	3.71	605	3.73	238.74	64.40	0.32	13.50
Lower	2133	3.24	3.58	8.87	1.97	4.50	512	2.06	273.77	60.80	0.29	12.45
Lower	2181	2.24	4.45	7.63	1.89	4.04	550	2.74	340.63	84.38	0.37	12.08

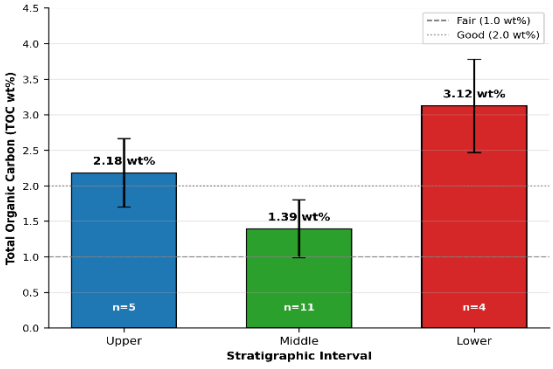


Figure 1: TOC percentage distribution showing stratigraphic variation across Upper, Middle, and Lower Maastrichtian intervals. Error bars represent ±1 standard deviation.

Hydrogen index (HI) and oxygen index (OI)

HI, reflecting kerogen hydrogen richness and oil potential, ranges from 195.51–601.03 mg HC/g TOC overall (Table 2; Fig. 2a). Upper Maastrichtian HI is 197.97–275.00 (mean 241.26 ± 31.31), indicating Type II/III mixed kerogen. Middle Maastrichtian shows the widest range (195.51–601.03; mean 349.60 ± 129.43), suggesting predominantly Type II oil-prone kerogen at depth and Type III gas-prone kerogen shallower. Lower Maastrichtian HI is 210.03–340.63 (mean 265.73 ± 55.09), consistent with Type II/III kerogen.

DOI: https://doi.org/10.53704/fujnas.v15i2.1572

Rock-Eval S1, S2, and S3 parameters

S1 (free hydrocarbons) ranges 1.09–4.73 mg HC/g rock (Table 2; Fig. 3): Upper 1.44–1.70 (mean 1.59 ± 0.11), middle 1.09–2.58 (mean 1.79 ± 0.49), and Lower 3.58–4.73 (mean 4.29 ± 0.51)—the elevated Lower-interval S1 values indicate high free-hydrocarbon contents, which may include a contribution from migrated hydrocarbons. S2 (generative potential) ranges 3.03–9.12 mg HC/g rock: Upper 4.40–5.86 (mean 5.15 ± 0.54), middle 3.03–6.25 (mean 4.53 ± 1.11), Lower 6.70–9.12 (mean 8.08 ± 1.09), indicating substantial remaining potential in the Lower interval despite advanced maturity. S3 (pyrolysis CO_2) ranges from 0.18–2.46 mg CO_2/g rock: Upper 0.65–1.01 (mean 076 ± 0.16), Middle 0.18–0.83 (mean 0.51 ± 0.20), and Lower 1.89–2.46 (mean 2.08 ± 0.27), with the elevated Lower-interval S3 suggesting greater terrigenous organic matter input.

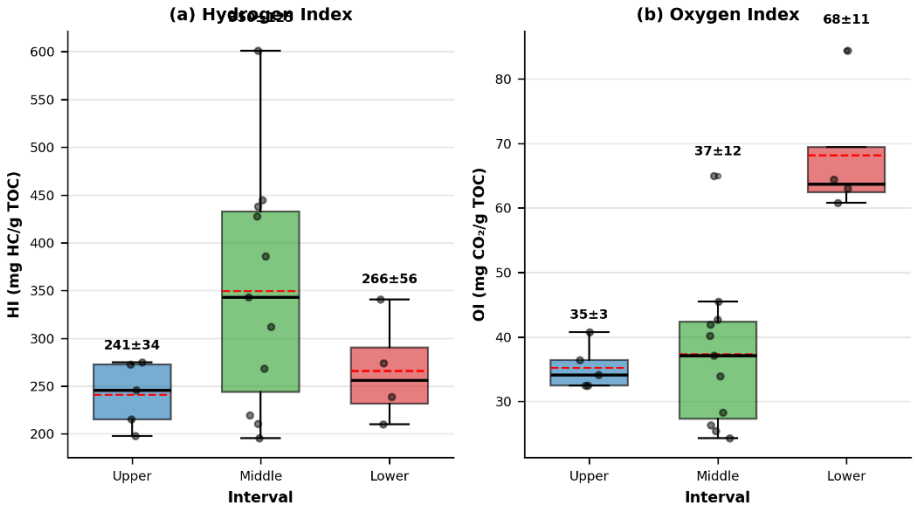


Figure 2: Hydrogen index (HI) and oxygen index (OI) values showing distribution across stratigraphic intervals. Error bars represent ±1 standard deviation.

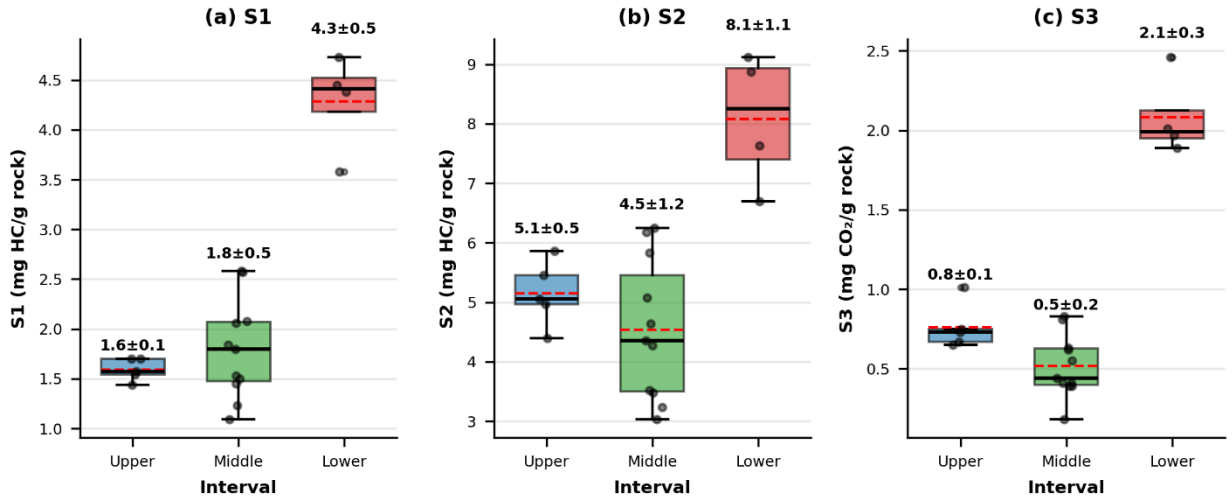


Figure 3: S1, S2, and S3 values for the Maastrichtian Dahomey Basin shales showing distribution across stratigraphic intervals. Error bars represent ±1 standard deviation.

Petroleum source potential (S1 + S2)

S1+S2 ranges 4.12–13.50 mg HC/g rock (Table 2; Figs. 4–5): Upper 5.97–7.40 (mean 6.73 ± 0.56, good–very good), middle 4.12–8.82 (mean 6.32 ± 1.51, fair–good, with notable intra-interval variability), and Lower 11.43–13.50 (mean 12.36 ± 0.88), consistently very good, with the maximum (13.50, at 2100 m) coincident with peak TOC. All intervals show good hydrocarbon-generation potential, but the Lower Maastrichtian is clearly best and has the highest proportion of very-good-quality samples (Fig. 5). S1 values, however, are also high in the Lower Maastrichtian (3.58–4.73 mg HC/g rock, all above the possible migrated hydrocarbons threshold of S1>1 mg/g) and indicate

DOI: https://doi.org/10.53704/fujnas.v15i2.1572

that part of the free hydrocarbons are not generated in situ but migrated, making S1+S2 values an overestimation of the real source-rock quality of this interval. Even with migrated hydrocarbons, the lower Maastrichtian interval in this well remains the best source-rock interval because it has higher remaining potential (mean S2 = 8.08 mg HC/g rock) than the upper (5.15) and middle (4.53) intervals.

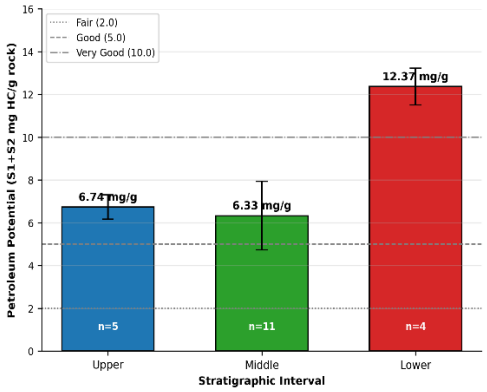


Figure 4: Petroleum source potential (S1+S2) values showing distribution across stratigraphic intervals. Error bars represent ±1 standard deviation.

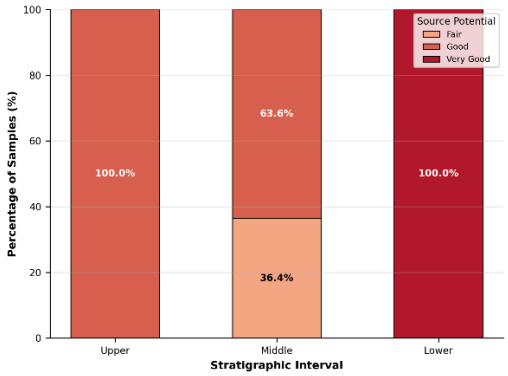


Figure 5: Percentage distribution of petroleum source potentials across Upper, Middle, and Lower Maastrichtian intervals.

S2/S3 Ratio

S2/S3, indicating likely expelled product type where kerogen type is known, ranges from 3.33–18.00 (Table 2): Upper 5.80–8.38 (mean 6.88 ± 1.03), Middle 4.30–18.00 (mean 9.85 ± 3.98), Lower 3.33–4.50 (mean 3.90 ± 0.49). Higher middle/Upper ratios indicate better liquid-hydrocarbon potential, while lower lower-interval ratios reflect more gas-prone/mixed organic matter consistent with advanced maturity.

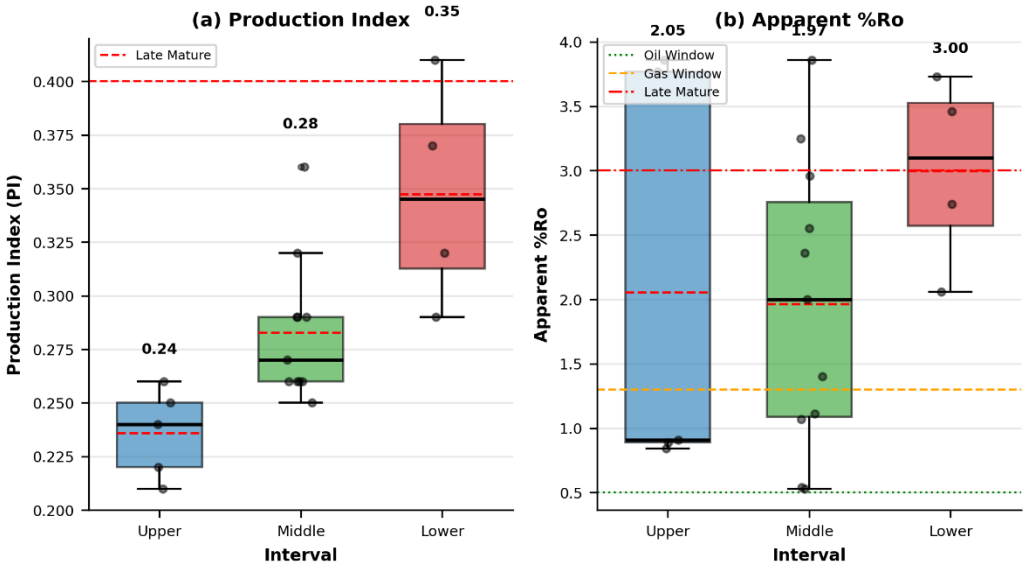


Figure 6: Production index (PI) and Tmax-derived apparent vitrinite reflectance (%Ro) values for the Maastrichtian Dahomey basin shales. Error bars represent ±1 standard deviation.

Production index (PI)

PI ranges 0.21–0.41 (Table 2; Fig. 6): Upper 0.21–0.26 (mean 0.23 ± 0.02), middle 0.25–0.36 (mean 0.28 ± 0.03), Lower 0.29–0.41 (mean 0.34 ± 0.05), indicating increasing kerogen-to-hydrocarbon conversion with depth/age. PI > 0.4 marks the late-mature stage [5]; Lower Maastrichtian samples approach this threshold.

Thermal maturity (Tmax and Tmax-derived apparent %Ro)

Tmax ranges 427–612°C (Table 2; Fig. 7): Upper 445–612°C (mean 512.0 ± 79.2), middle 427–612°C (mean 507.0 ± 63.3), Lower 512–605°C (mean 564.3 ± 41.8). The wide late/middle range spans immature (427°C, shallowest middle sample) to early-

DOI: https://doi.org/10.53704/fujnas.v15i2.1572

mature/late mature (>470°C, deeper samples), while Lower Maastrichtian samples consistently fall in the mature-to-late mature window, with the highest proportion of peak-mature to late mature samples (Fig. 7).

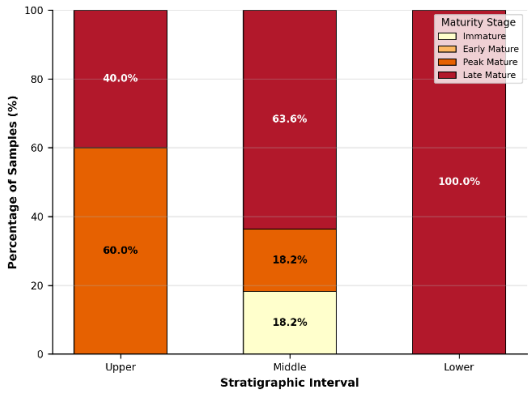


Figure 7: Average percentage distribution of Tmax values across the Maastrichtian stratigraphic horizons showing thermal maturity categories.

Tmax-derived apparent vitrinite reflectance %Ro [31] ranges 0.53–3.86% (Table 2; Fig. 8): Upper mean 2.05 ± 1.42%, middle mean 1.97 ± 1.14%, Lower mean 3.00 ± 0.70%, spanning the oil window (0.5–1.3 Tmax-derived apparent %Ro) through the gas window (1.3–3.0 Tmax-derived apparent %Ro) and, in some samples, exceeding 3.0% apparent %Ro. These values are treated as indicative of relative maturity trends rather than as precise measurements, and the term 'late mature' is used only as a descriptive label for apparent %Ro >3.0%.

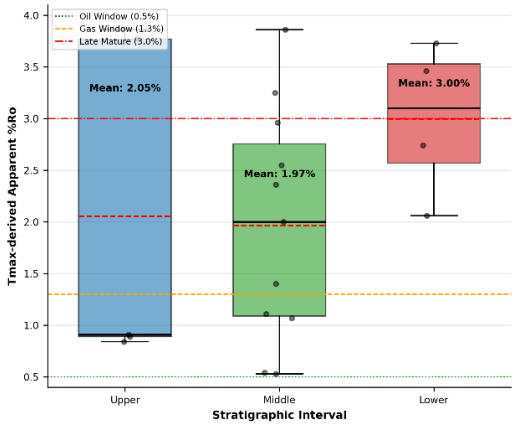


Figure 8: Tmax-derived apparent vitrinite reflectance (%Ro) values showing distribution across stratigraphic intervals. Error bars represent ±1 standard deviation.

Kerogen type classification

Kerogen types were determined from HI–OI (Van Krevelen; Fig. 9) and S2–TOC (Fig. 10) cross-plots [5]. Upper Maastrichtian samples (WX-01–WX-05) plot mainly in the Type II/III field, HI 197.97–275.00 (mean 241.29) and OI 32.47–40.78 mg CO_2/g TOC (mean 35.26), with one sample (WX-01, 1128 m) showing Type III character. The Middle Maastrichtian shows the greatest kerogen variability, spanning Type III at shallow depth (e.g., WX-06, 1287 m: HI 195.51, OI 45.51) through Type II/III mixed (WX-07, WX-08) to Type II oil-prone; notably, WX-11 (1578 m) shows Type I character (HI 601.03, OI 64.95), suggestive of algal-rich organic matter. Lower Maastrichtian samples (WX-17–WX-20) plot predominantly Type II/III, HI 210.03–340.63 (mean 265.79) and OI 60.80–84.38 (mean 68.15); despite elevated OI indicating terrigenous input, HI remains high enough for mixed marine-terrigenous oil/gas potential, with WX-20 (2181 m) showing clear Type II character. The S2–TOC plot (Fig. 10) confirms Lower Maastrichtian samples have the highest S2 yield relative to TOC, indicating the best overall source quality.

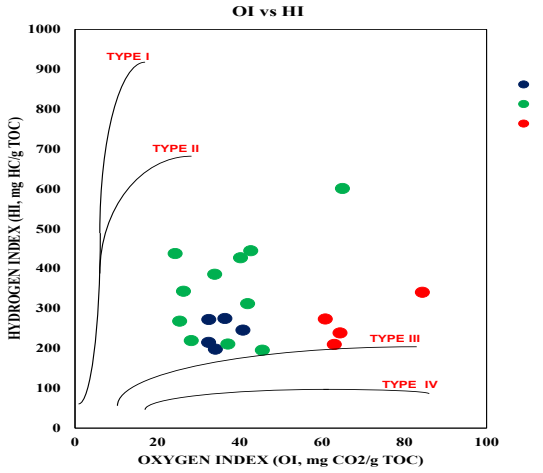


Figure 9: Van Krevelen's hydrogen index versus oxygen index plot showing kerogen type constituents of the studied source rocks.

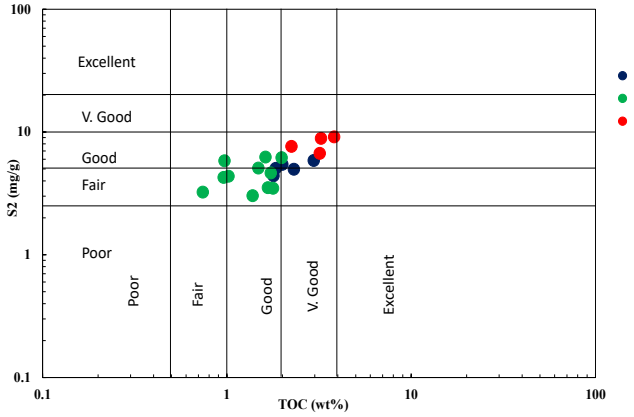


Figure 10: Hydrogen yield (S2 kg/t) versus TOC (wt%) of the studied shales, used for source-rock type evaluation.

DOI: https://doi.org/10.53704/fujnas.v15i2.1572

Depth relationships

Relationship of Tmax-derived apparent vitrinite reflectance (%Ro) to depth

Tmax-derived apparent %Ro shows substantial scatter with depth, and the linear relationship is weak and non-significant (R^2 = 0.079, p = 0.229; Fig. 11). Mean apparent %Ro values are 2.05% for the Upper interval, 1.97% for the Middle interval, and 3.00% for the Lower interval. Although the Lower interval records the highest mean apparent %Ro, the data do not demonstrate a consistent linear increase in apparent maturity with depth. The wide within-interval variability indicates that factors beyond burial depth may influence apparent maturity values.

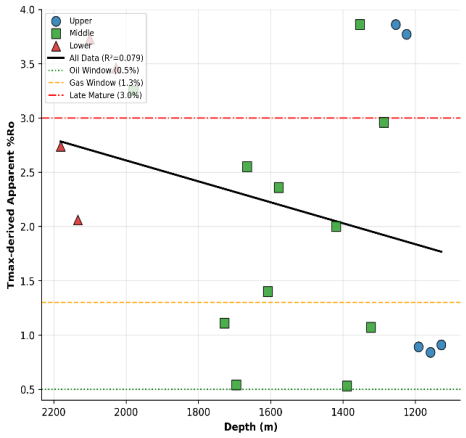


Figure 11: Relationship between depth and Tmax-derived apparent %Ro, showing substantial scatter and a weak, non-significant linear depth trend (R^2 = 0.079, p = 0.229).

Relationship of depth to hydrocarbon potentiality (S1+S2)

S1+S2 (4.12–13.50 mg HC/g rock) shows a moderate positive relationship with burial depth (R^2 = 0.387; Fig. 12), with mean values of 6.74 ± 0.56 mg HC/g rock in the Upper interval, 6.33 ± 1.51 mg HC/g rock in the Middle interval, and 12.37 ± 0.88 mg HC/g rock in the Lower interval. The higher S1+S2 values at greater depth largely reflect the greater organic richness and higher S2 values of the Lower Maastrichtian. However, the elevated S1 values in this interval may partly represent migrated hydrocarbons; therefore, the depth–S1+S2 relationship should not be interpreted solely in terms of in-situ generation and maturation.

Statistical analysis

Multivariate analyses were performed on the Rock-Eval/TOC dataset to evaluate geochemical differentiation among the depth-defined intervals and identify the primary controls on source-rock quality.

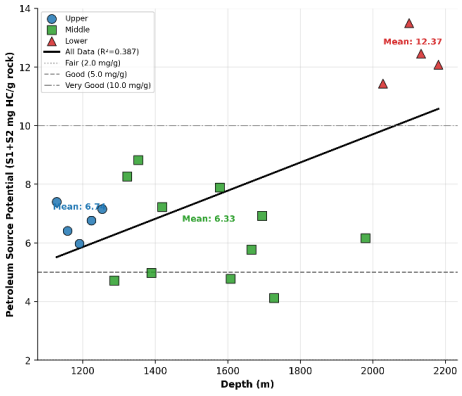


Figure 12: Depth vs. S1+S2 potential showing the relationship between burial depth and hydrocarbon generation potential.

Analysis of variance (ANOVA)

One-way ANOVA (Table 3) shows highly significant differences (p < 0.01; F = 6.57–93.71) between intervals for TOC, S1, S2, S3, OI, S2/S3, PI, and S1+S2. Levene's test confirmed homogeneity of variance for all parameters (p > 0.05) except S1+S2 (p = 0.036), for which Welch's ANOVA was used (Welch's F = 63.80, p < 0.001) with Games-Howell post-hoc tests. The exceptionally high F for S3 (93.71, p < 0.001) reflects the marked increase in terrigenous input in the Lower Maastrichtian. The strong differences observed for S3 (F = 93.71, p < 0.001), S1+S2 (Welch's F = 63.80, p < 0.001), and TOC (F = 20.05, p < 0.001) further demonstrate substantial vertical geochemical variation among the studied intervals. Tmax and Tmax-derived apparent %Ro do not differ significantly among the depth-defined intervals (p > 0.05), and their substantial within-interval variability is consistent with the absence of a strong linear maturity trend with depth

Post-hoc comparisons (Table 4) show that TOC differs significantly among all three intervals, with the Lower Maastrichtian having the highest mean, followed by the Upper and then the Middle interval (Lower > Upper > Middle). For S1 and S2, the Lower interval is significantly higher than both the Middle and Upper intervals, whereas the Middle and Upper intervals do not differ significantly. S3 and OI are also significantly higher in the Lower interval than in the other two intervals. PI is significantly higher in the Lower intervals than in both the Middle and Upper intervals. For S2/S3, only the Lower–Middle comparison is significant, with the Middle interval having the higher ratio. Because S1+S2 violated the homogeneity-of-variance assumption, Games–Howell comparisons were used; these show that the

DOI: https://doi.org/10.53704/fujnas.v15i2.1572

Lower interval is significantly higher than both the Middle and Upper intervals, while the Middle and Upper intervals do not differ significantly. The size of these differences is supported by effect sizes (η^2 and ω^2). The largest conventional ANOVA effect sizes were observed for S3 ($\eta^2 = 0.92$, $\omega^2 = 0.91$) and S1 ($\eta^2 = 0.87$, $\omega^2 = 0.85$). S1+S2 was analysed separately using Welch's ANOVA because the homogeneity-of-variance assumption was violated. Welch's ANOVA confirmed a highly significant difference in S1+S2 among the depth-defined intervals (Welch's $F(2, 8.55) = 63.80$, $p < 0.001$). Moderate to large effects were observed for TOC ($\eta^2 = 0.70$), S2 ($\eta^2 = 0.66$), OI ($\eta^2 = 0.64$), and PI ($\eta^2 = 0.57$). Tmax, HI, and apparent %Ro showed no significant differences among the depth-defined intervals ($p = 0.350$, 0.118, and 0.350, respectively), with η^2 values ranging from 0.12 to 0.22, reflecting substantial within-group variability.

Table 3: One-way ANOVA results for geochemical parameters among the Lower, Middle and Upper depth-defined Maastrichtian intervals.

Parameter	SS_between	df_between	MS_between	SS_within	df_within	MS_within	F-statistic	p-value	η^2	ω^2	Levene's p	Test Used	Significant
TOC	13.51	2	6.75	5.79	17	0.34	20.05	<0.001	0.70	0.67	0.918	A	Yes
S1	19.49	2	9.75	3.01	17	0.18	55.11	<0.001	0.87	0.85	0.127	A	Yes
S2	18.08	2	9.04	9.13	17	0.54	16.83	<0.001	0.66	0.63	0.190	A	Yes
S3	6.99	2	3.50	0.63	17	0.04	93.71	<0.001	0.92	0.91	0.720	A	Yes
Tmax	5272.90	2	2636.45	40086.90	17	2358.05	1.12	0.350	0.12	0.02	0.624	A	No
HI	17610.26	2	8805.13	61763.34	17	3633.14	2.42	0.118	0.22	0.14	0.050	A	No
OI	1321.59	2	660.80	755.71	17	44.45	14.86	<0.001	0.64	0.60	0.278	A	Yes
S2/S3	86.34	2	43.17	111.68	17	6.57	6.57	0.008	0.44	0.37	0.101	A	Yes
PI	0.017	2	0.008	0.013	17	0.0007	11.19	<0.001	0.57	0.52	0.213	A	Yes
S1+S2	—	2[1]	—	—	8.55[1]	—	63.80	<0.001	—	—	0.036	W	Yes
Apparent %Ro	2.37	2	1.18	17.96	17	1.06	1.12	0.350	0.12	0.02	0.624	A	No

Key: A = One-way ANOVA; W = Welch's ANOVA

NOTE: A = one-way ANOVA; W = Welch's ANOVA. For S1+S2, Levene's test indicated unequal variances ($p = 0.036$); therefore, Welch's ANOVA was used. The reported degrees of freedom (2 and 8.55) are the Welch numerator and denominator degrees of freedom, respectively. Conventional sums of squares, mean squares, η^2, and ω^2 are not reported for this row because they do not form the basis of the Welch F statistic. All other parameters were analysed using standard one-way ANOVA with df = 2, 17.

Table 4: Post-hoc pairwise comparisons of geochemical parameters among depth-defined Maastrichtian intervals.

Parameter	Comparison	Mean difference[1]	SE	Test statistic	p-value	Significant	Post-hoc test
TOC	Lower – Middle	1.7289	0.2791	6.1940	<0.001	Yes	Tukey HSD
	Lower – Upper	0.9425	0.3207	2.9391	0.0236	Yes	Tukey HSD
	Middle – Upper	−0.7864	0.2578	−3.0498	0.0188	Yes	Tukey HSD
S1	Lower – Middle	2.4914	0.2550	9.7683	<0.001	Yes	Tukey HSD
	Lower – Upper	2.6950	0.2930	9.1971	<0.001	Yes	Tukey HSD
	Middle – Upper	0.2036	0.2356	0.8643	0.6693	No	Tukey HSD
S2	Lower – Middle	3.5455	0.6145	5.7700	<0.001	Yes	Tukey HSD
	Lower – Upper	2.9320	0.7060	4.1532	0.0018	Yes	Tukey HSD
	Middle – Upper	−0.6135	0.5676	−1.0807	0.5384	No	Tukey HSD
S3	Lower – Middle	1.5680	0.1154	13.5877	<0.001	Yes	Tukey HSD
	Lower – Upper	1.3205	0.1326	9.9601	<0.001	Yes	Tukey HSD
	Middle – Upper	−0.2475	0.1066	−2.3214	0.0798	No	Tukey HSD
OI	Lower – Middle	30.8084	6.0406	5.1002	<0.001	Yes	Tukey HSD
	Lower – Upper	32.8915	6.9402	4.7393	<0.001	Yes	Tukey HSD
	Middle – Upper	2.0831	5.5801	0.3733	0.9264	No	Tukey HSD
S2/S3	Lower – Middle	−5.9623	1.7008	−3.5055	0.0072	Yes	Tukey HSD
	Lower – Upper	−2.9830	1.9541	−1.5265	0.3038	No	Tukey HSD
	Middle – Upper	2.9793	1.5712	1.8962	0.1701	No	Tukey HSD
PI	Lower – Middle	0.0648	0.0205	3.1554	0.0151	Yes	Tukey HSD
	Lower – Upper	0.1115	0.0236	4.7277	<0.001	Yes	Tukey HSD
	Middle – Upper	0.0467	0.0190	2.4642	0.0608	No	Tukey HSD
S1+S2	Lower – Middle	6.0368	0.6485	9.3083	<0.001	Yes	Games–Howell
	Lower – Upper	5.6270	0.5029	11.1900	<0.001	Yes	Games–Howell
	Middle – Upper	−0.4098	0.5462	−0.7503	0.738[2]	No	Games–Howell

NOTE: [1] Mean difference = mean of the first interval minus mean of the second interval. A positive value indicates the first interval has the higher mean; a negative value indicates the first interval has the lower mean. [2] The manuscript reports approximately p = 0.738 for the Middle–Upper Games–Howell comparison. S1+S2 was analysed using Games–Howell because homogeneity of variance was violated (Levene's p = 0.036). All other parameters shown were analysed using Tukey HSD following the corresponding significant omnibus ANOVA.

DOI: https://doi.org/10.53704/fujnas.v15i2.1572

Pearson correlation analysis

Correlation analysis (Fig. 13) shows very strong positive correlations between S1+S2 and TOC (r = 0.76), S1 (r = 0.94), and S2 (r = 0.97), confirming organic-matter abundance and quality as the primary controls on generation potential. TOC also correlates strongly with S3 (r = 0.88), supporting increased terrigenous input in the Lower Maastrichtian shales. Conversely, TOC correlates negatively with HI (r = –0.62) and S2/S3 (r = –0.74), indicating that as organic richness increases, kerogen hydrogen-richness diminishes—typical of Type II/III mixed kerogen where higher TOC is accompanied by more oxygen-bearing terrigenous components. Tmax and Tmax-derived apparent %Ro display a near-perfect positive correlation (r = 0.999). This correlation is mathematically inherent because apparent %Ro is calculated directly from Tmax using the Jarvie et al. [31] equation, and it therefore does not constitute independent validation of either parameter.

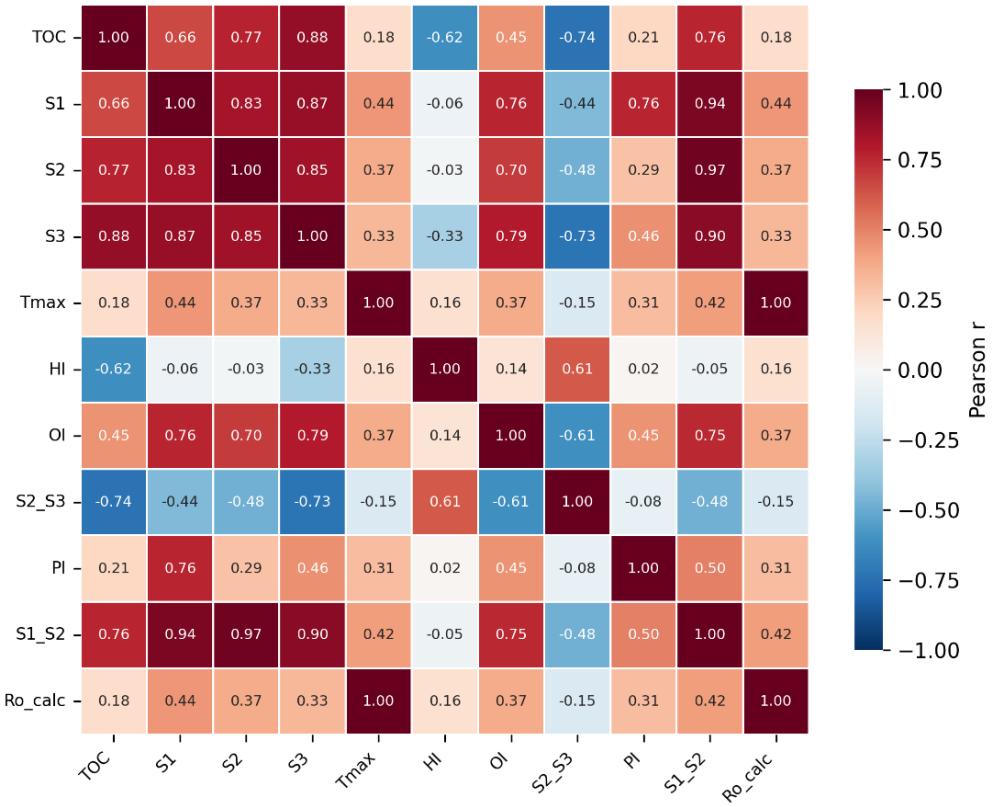


Figure 13: Pearson correlation matrix

Principal component analysis (PCA)

The first two principal components (PC1 and PC2) together explain 75.1% of the total variance (PC1 = 53.7%, PC2 = 21.4%), and this two-component model is used for interpretation. A third component (PC3) explains an additional 12.1%, bringing the cumulative variance to 87.2%, but it is not used for primary geochemical interpretation because it is not represented in the 2D biplot (Fig. 16). The loading matrix (Table 5) shows PC1 is strongly positively loaded by S1, S3, S2, OI, and TOC (organic richness/productivity axis), and PC2 is heavily positively loaded by HI, Tmax, and Tmax-derived %Ro (kerogen quality/thermal maturity axis). The 3D scatter (Fig. 15) and 2D biplot (Fig. 16) show clear separation by interval: Lower Maastrichtian samples (WX-17–WX-20) cluster distinctly in the positive PC1 region, driven by elevated TOC, S1, S2, and S3, and are strongly associated with the S3 and OI vectors, confirming mixed marine-terrigenous input. Middle Maastrichtian samples scatter widely along PC2, reflecting highly variable kerogen quality (Type III to Type I), while Upper Maastrichtian samples occupy an intermediate position with moderate richness and Type II/III kerogen. This pattern mirrors successful multivariate source-rock prediction in other West African basins using TOC, S2, and S3 [36, 17]. It should be noted that Tmax and apparent %Ro are mathematically related (r = 0.999), and their loadings on PC2 are therefore not independent. This collinearity is a limitation of the PCA presented here. Because Tmax and apparent %Ro are mathematically dependent, their joint inclusion may

DOI: https://doi.org/10.53704/fujnas.v15i2.1572

overweight the maturity contribution to PC2; consequently, the maturity-related interpretation of PC2 is treated cautiously.

Table 5: PCA loading matrix showing the contribution of each geochemical parameter to the first three principal components.

Parameter	PC1 Loading	PC2 Loading	PC3 Loading
TOC	0.346	-0.411	-0.251
S1	0.432	-0.009	0.222
S2	0.397	-0.096	0.071
S3	0.426	-0.220	0.028
HI	-0.066	0.537	0.504
OI	0.368	0.061	0.328
Tmax	0.266	0.482	-0.442
PI	0.272	0.129	0.361
Apparent_Ro	0.265	0.482	-0.441

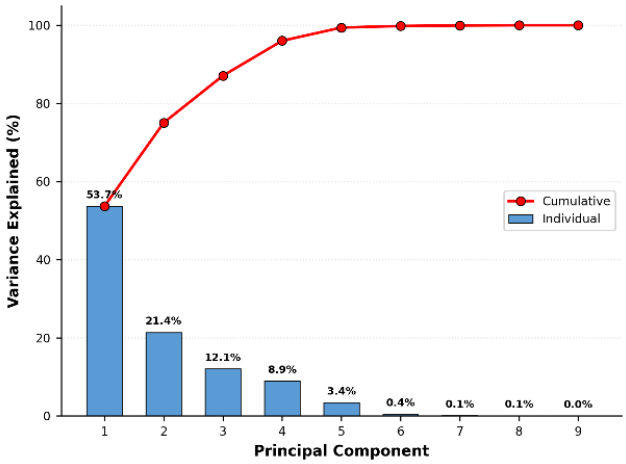


Figure 14: Scree plot showing individual and cumulative explained variance of the first nine principal components.

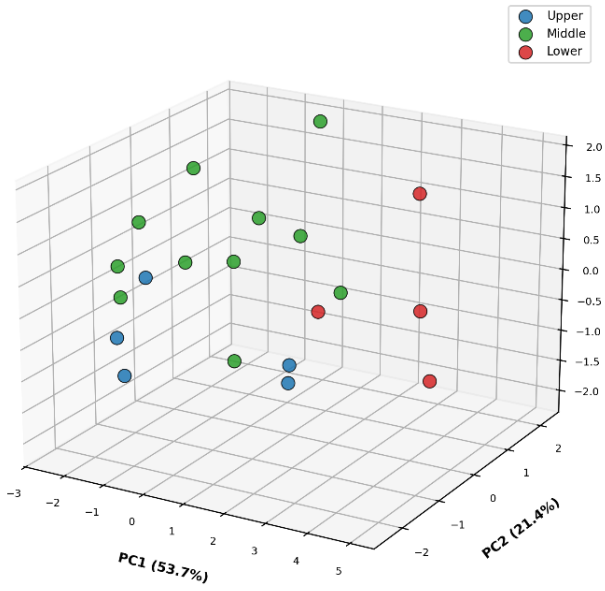


Figure 15: 3D PCA scatter plot showing sample distribution by stratigraphic interval.

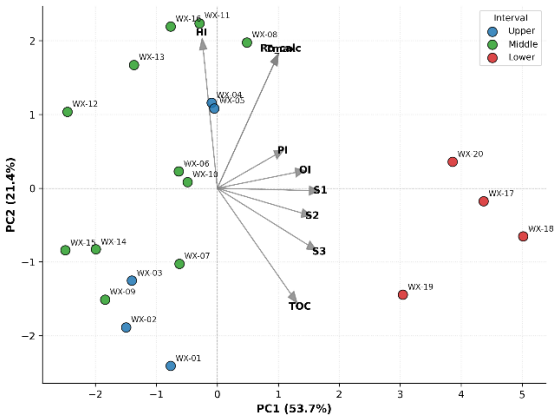


Figure 16: 2D PCA biplot illustrating the relationship between samples and geochemical variable vectors.

Hierarchical cluster analysis (HCA) and K-Means clustering

The elbow method (Fig. 17) and inspection of the hierarchical-clustering dendrogram (Fig. 18) indicated that a three-cluster representation could provide a useful exploratory description of the geochemical variability within the studied succession. However, silhouette analysis favoured a two-cluster solution, with a mean silhouette coefficient of 0.4638 for k = 2 compared with 0.3646 for k = 3, indicating better statistical compactness and separation for two clusters. Consequently, the k = 3 solution is retained here as a stratigraphically informed exploratory representation rather than the statistically optimal clustering solution. In the three-cluster K-means solution, all four Lower-interval samples form a distinct cluster characterised by the highest mean TOC (3.12 wt%), S1 (4.29 mg HC/g rock), S2 (8.08 mg HC/g rock), S3 (2.08 mg CO_2/g rock), and S1+S2 (12.37 mg HC/g rock). In contrast, samples from the Upper and Middle intervals are distributed between the remaining two clusters, demonstrating substantial geochemical overlap between these intervals. Thus, the clustering most clearly distinguishes the Lower interval, whereas the Upper and Middle intervals display greater internal heterogeneity and less distinct statistical separation. This pattern is consistent with the broader observation that Cretaceous source rocks may exhibit substantial vertical geochemical heterogeneity, as also reported from the Tano Basin of Ghana [36]. The cophenetic correlation coefficient for the Ward-linkage dendrogram was 0.8743, indicating that the dendrogram well represents pairwise dissimilarities in the original geochemical dataset. This coefficient supports the fidelity of the hierarchical representation but does not, by itself, establish that three clusters constitute the statistically optimal

DOI: https://doi.org/10.53704/fujnas.v15i2.1572

solution. Overall, the clustering analyses provide evidence for pronounced vertical geochemical heterogeneity and particularly strong differentiation of the Lower interval; however, they do not independently validate the Lower, Middle, and Upper depth-defined intervals as three discrete chronostratigraphic or geochemical units.

Table 6: K-means cluster centres showing the mean geochemical values for the exploratory k = 3 solution.

Cluster	TOC	S1	S2	S3	HI	OI	Tmax	PI	Ro_calc
0 (mostly Middle)	1.46	1.79	4.96	0.59	371.73	42.32	577.14	0.264	3.23
1 (mostly Upper/Mid)	1.78	1.68	4.55	0.59	272.30	32.31	455.22	0.271	1.03
2 (mostly Lower)	3.12	4.29	8.08	2.08	265.79	68.15	564.25	0.348	3.00

Table 7: K-Means cluster membership for individual samples (WX-01 to WX-20)

Sample ID	Depth (m)	Depth-defined interval	K-means cluster
WX-01	1128	Upper	1
WX-02	1158	Upper	1
WX-03	1191	Upper	1
WX-04	1224	Upper	0
WX-05	1254	Upper	0
WX-06	1287	Middle	0
WX-07	1323	Middle	1
WX-08	1353	Middle	0
WX-09	1389	Middle	1
WX-10	1419	Middle	1
WX-11	1578	Middle	0
WX-12	1608	Middle	1
WX-13	1665	Middle	0
WX-14	1695	Middle	1
WX-15	1728	Middle	1
WX-16	1980	Middle	0
WX-17	2028	Lower	2
WX-18	2100	Lower	2
WX-19	2133	Lower	2
WX-20	2181	Lower	2

Cluster labels are arbitrary numerical identifiers and do not represent stratigraphic order. The k = 3 solution is presented for exploratory geological interpretation; silhouette analysis identified k = 2 as the statistically better-separated solution.

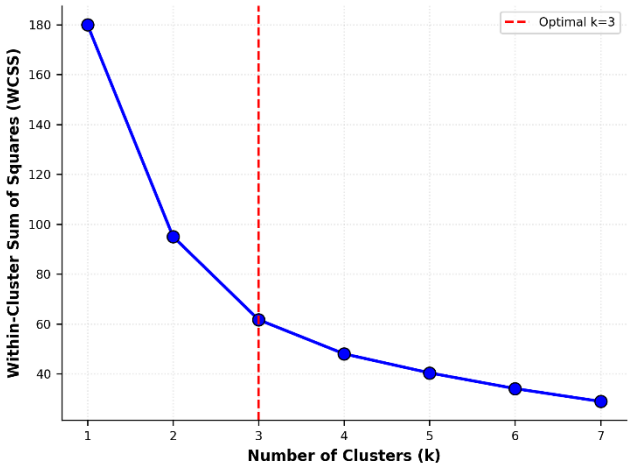


Figure 17: Elbow-method plot used to evaluate the number of K-means clusters.

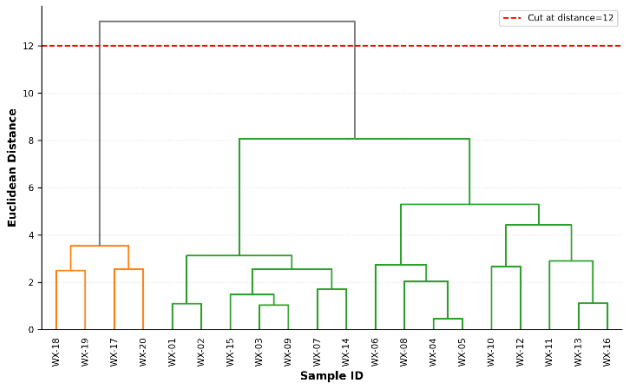


Figure 18: Hierarchical clustering dendrogram showing sample groupings.

Discussion

The Maastrichtian shales of the Araromi Formation are stratigraphically highly variable in organic matter content, ranging from 0.74 to 3.82 wt% TOC. The increase in mean TOC from the Upper to the Lower Maastrichtian (Fig. 1) reflects variations in organic-matter supply, productivity, dilution, and preservation. This variability is typical of marine source rocks, and enrichment reflects productivity,

DOI: https://doi.org/10.53704/fujnas.v15i2.1572

sedimentation rate, redox conditions, and preservation efficiency [4, 5]. The higher TOC in the Lower Maastrichtian aligns with increased organic accumulation during the marine transgression. Upper Cretaceous strata in the eastern Dahomey Basin record recurrent transgressive and highstand phases [24], and Araromi sediments were deposited in a coastal, brackish-water, shallow-marine environment [22]. This is further corroborated by the foraminiferal and palynomorph assemblages, which indicate a marine environment with varying degrees of continental influence [24, 37].

The Lower Maastrichtian interval also shows higher OI (mean of 68.15 mg CO_2/g TOC) and S3 (mean of 2.08 mg CO_2/g rock) than the Upper and Middle intervals (Figs. 2b and 3c), indicating greater input of oxygen-rich organic matter from land. This is consistent with the presence of higher plant material on top of marine organic matter, since the OI of lipid-rich marine organic matter is generally lower than that of lignocellulosic terrestrial material [1, 4, 30]. Moreover, recent geochemical data show that continental sediment supply and weathering were variable during Cretaceous sedimentation in the Dahomey Basin [38].

The Middle Maastrichtian shows the highest overall variability in TOC (0.74-1.98 wt%), HI (195.51-601.03 mg HC/g TOC), and OI (24.32-64.95 mg CO_2/g TOC), with the widest PCA scatter and distribution across multiple K-Means clusters. The occurrence of Type I character in WX-11, alongside Type II/III and III samples, indicates variation in aquatic and terrestrial organic inputs, likely reflecting a dynamic marginal- to shallow-marine environment, sea-level fluctuations, productivity, and clastic influx [24, 22]. Very low TOC values, such as 0.74 wt% in WX-12, may reflect dilution, poorer preservation, or oxidation under more oxygenated conditions [39]. Upper Maastrichtian shales are more uniform and mostly type II/III, reflecting relatively balanced marine and terrestrial input and transitional coastal (to shallow marine) deposition [6, 22].

Based on the Van Krevelen diagram (Fig. 9) and the S2–TOC plot (Fig. 10), most organic matter is Type II/III mixed kerogen, with subordinate Type II, Type III, and locally Type I organic matter. This reflects different contributions from marine algal/planktonic and terrestrial higher plants. Type II/III kerogen is mixed oil- and gas-generative; Type II kerogen is more oil-prone, and Type III is more gas-prone [4, 5]. Mixed organic facies similar to those observed here have been reported from the Nigerian Cretaceous source rocks [40].

Average S1+S2 for the Lower (12.36 mg HC/g rock), Upper (6.73 mg HC/g rock) and Middle (6.32 mg HC/g rock) intervals (Fig. 4) indicate that the Lower interval has the most potential. Conventional screening indicates high generative potential in the Lower Maastrichtian and good to very good generative potential elsewhere [5]. However, petroleum generation depends on kerogen quality, maturity, expulsion, migration, and preservation. Although TOC and S1+S2 are higher in the lower Lower Maastrichtian, the HI (265.73 mg HC/g TOC) is lower than in the Middle interval (349.60 mg HC/g TOC), indicating more terrestrial influence and hydrogen-poor marine organic matter [32] diluting the hydrogen-rich marine organic matter.

A few Middle Maastrichtian samples contain oil-prone Type II kerogen, including WX-08 and WX-13, and WX-11 has a very high HI (601.03 mg HC/g TOC), suggesting an enrichment in hydrogen-rich organic matter. This variation may reflect aquatic productivity, preservation, marine influence, and terrestrial input [41, 40]. The mean S2/S3 is lowest in the Lower Maastrichtian (3.90), highest in the Middle Maastrichtian (9.85), and intermediate in the Upper Maastrichtian (6.88), indicating greater oil-generative potential in parts of the Middle Maastrichtian. The geochemistry of the Araromi Formation is thus heterogeneous, not uniformly oil- or gas-prone as stated by Oluwajana et al. [22] and Aigbadon et al. [27].

The Tmax values (427–612°C) and Tmax-derived apparent vitrinite reflectance (%Ro; 0.53–3.86%) indicate maturity ranging from immature to late mature, based on apparent %Ro trends and consistent with the measured Tmax values (Figs. 7–8). Samples at 2028–2181 m have an average Tmax-derived apparent vitrinite reflectance %Ro of 3.00% and are most thermally advanced in the Lower Maastrichtian. The Lower interval records the highest mean Tmax-derived apparent %Ro (Fig. 11); however, apparent %Ro shows considerable scatter throughout the well and does not exhibit a statistically significant linear relationship with depth. Consequently, the higher mean apparent maturity indicators in the Lower interval should not be interpreted as evidence of a simple progressive burial-related maturity trend. Basin modelling also indicates that the deeper portions of the Dahomey Basin are more mature and contain more hydrocarbons than the shallow onshore sections [18,27]. Note that Tmax-derived %Ro was

DOI: https://doi.org/10.53704/fujnas.v15i2.1572

calculated, and the extremely high Tmax and Tmax-derived apparent vitrinite reflectance %Ro values indicate high thermal evolution rather than precise maturity measurements. Although the Lower interval records the highest mean apparent maturity indicators, the substantial within-interval scatter in Tmax and Tmax-derived apparent %Ro indicates that maturity cannot be explained by burial depth alone. The Lower Maastrichtian records high apparent maturity indicators; however, the anomalously high Tmax values and absence of directly measured vitrinite reflectance prevent definitive assignment to a post-oil-window maturity stage. S1+S2 shows a moderate positive relationship with burial depth (R^2 = 0.387; Fig. 12), with the deeper Lower interval recording the highest values. This pattern is more consistent with the greater organic richness and higher S2 of the Lower interval than with a simple progressive depletion of generative potential through maturation and expulsion [4, 5].

The Middle Maastrichtian shows the widest maturity range, from WX-09 (apparent %Ro = 0.53%, the least mature sample in the dataset) to samples exceeding 3% apparent %Ro, while the Upper Maastrichtian spans the oil window to late-mature conditions. This wide range indicates that maturity within the middle interval is heterogeneous and influenced by factors beyond simple burial depth. This variability suggests that stratigraphic position, burial history, heat flow, structural setting, and organic-matter composition affect maturity. Such spatial variation in burial and thermal history is possible in the Dahomey Basin, where faulting controls a horst-and-graben architecture [42]. The samples in this study are significantly more mature than the shallow Araromi sediments, which have been previously demonstrated to host thermally immature Type III–IV organic matter [22]. This contrast indicates that burial depth strongly influences source-rock effectiveness and aligns with basin models suggesting generation and migration from deeper mature kitchens [18, 27]. The regional bituminous sands also indicate an active petroleum system and migrating hydrocarbons from the deeper Cretaceous source rocks [43, 44].

A major outcome of this study is the pronounced vertical geochemical heterogeneity within the Maastrichtian succession. Statistical analyses (ANOVA, Tukey HSD, PCA, HCA, and K-Means) show significant differences among the depth-defined intervals for several geochemical parameters, with the Lower interval showing the clearest differentiation from the Middle and Upper intervals. According to ANOVA (Table 3), significant differences exist among the three intervals for TOC, S1, S2, S3, OI, S2/S3, PI and S1+S2 ($p<0.01$). The high-test statistics for S3 (F = 93.71), S1+S2 (Welch's F = 63.80), and TOC (F = 20.05) indicate pronounced differences among the depth-defined intervals for these parameters. Tmax and Tmax-derived apparent %Ro do not differ significantly among the three depth-defined intervals, reflecting substantial within-interval variability in these maturity indicators. Tukey HSD analysis (Table 4) shows significant differences in TOC among all three intervals, with the Lower interval having the highest mean, followed by the Upper and then the Middle interval (Lower > Upper > Middle) as reported by [35]. The Lower Maastrichtian S1+S2 is quite different from both the Middle and Upper intervals and represents the most organically enriched and generatively different interval. It also has high S3 and OI, indicating greater terrestrial influence. A similar vertical and lateral heterogeneity has been reported in the Cretaceous source rocks of the Dahomey and Tano basins [22, 45, 27].

These relationships are further resolved by PCA. PC1 accounts for 53.7% of the total variance and is dominated by TOC, S1, S2, S3 and OI, which are related to the organic richness and composition, while PC2 accounts for 21.4% and is related to HI, Tmax and Tmax-derived apparent vitrinite reflectance %Ro, which are related to kerogen quality and maturity. Together, they account for 75.1% of all the variance. Lower Maastrichtian samples are concentrated in the positive PC1 and S3/OI quadrant; Middle Maastrichtian samples show the greatest scatter, and Upper Maastrichtian samples lie in an intermediate position. In the exploratory k = 3 K-means solution, all four Lower-interval samples form Cluster 2, whereas Upper and Middle samples are distributed across Clusters 0 and 1. Thus, the multivariate analyses most clearly distinguish the Lower interval, while the Upper and Middle intervals show substantial geochemical overlap. These results support vertical geochemical heterogeneity within the succession but do not independently validate the three depth-defined intervals as discrete geochemical or chronostratigraphic units.

The Lower Maastrichtian is the most organically enriched interval and records the highest mean apparent maturity indicators, with mean S2 of 8.08 mg HC/g rock and elevated mean Tmax and Tmax-derived apparent %Ro. High S1 (3.58–4.73 mg HC/g rock)

DOI: https://doi.org/10.53704/fujnas.v15i2.1572

indicates partial hydrocarbon migration, so the mean S1+S2 of 12.37 mg HC/g rock reflects retained, migrated, and remaining hydrocarbons rather than a fully spent source rock. This aligns with petroleum-system models indicating that the deeper Cretaceous source rocks are in an effective generating window, while the shallow equivalents are immature [18, 27]. Type II/III kerogen with subordinate Type II, III, and locally Type I kerogen represents potential oil and gas generation, depending on organic facies and maturity. Intervals above the Higher-HI Middle Maastrichtian may be more favourable for liquids, whereas the Type III-rich intervals are comparatively gas-prone. Other petroleum systems in Nigeria and West Africa are similarly heterogeneous, including Cretaceous source rocks [40, 46, 45]. The positive depth–S1+S2 relationship, together with elevated S1 values in the deeper samples, emphasises the need to integrate source-rock richness, maturity, migration, and trapping when interpreting the petroleum system. The basin's horst-and-graben morphology suggests migration pathways and structural trapping [42]; depositional texture and diagenesis influence reservoir quality in Cretaceous–Paleogene sandstones [20]. Another piece of evidence for basin generation and migration is the widespread bituminous sand [44].

The significant stratigraphic variations observed in the ANOVA and multivariate analyses also have implications for petroleum-system modelling. Treating the entire Maastrichtian succession as a homogeneous source-rock unit would mask important variations in TOC, kerogen quality, maturity, and generative potential. Interval-specific properties must therefore be included in burial-history and generation models [18, 27]. Lastly, the Araromi Formation is part of the larger West African Transform Margin petroleum system where the Cretaceous source rocks are known to exhibit organic-facies and maturity heterogeneities [45]. The presence of mixed Type II/III kerogen, a mature and deep kerogen source kitchen, fault-controlled basin architecture, hydrocarbon migration and variable reservoir quality makes deeper and structurally favourable areas of the Dahomey Basin potential for further exploration [6, 20, 27].

Four samples (WX-04, WX-05, WX-08, and WX-18) yielded anomalously high Tmax values (>600°C), with corresponding Tmax-derived apparent %Ro values exceedingly approximately 3.7%. These values are unusually high relative to the burial depths of the samples and should therefore be interpreted cautiously. Repeat analyses indicated that the Tmax values were reproducible; nevertheless, they may reflect local thermal anomalies, reworked or altered organic matter, mineral-matrix effects, or other factors affecting Rock-Eval Tmax rather than regional thermal maturity alone. Accordingly, these anomalous Tmax and derived apparent %Ro values are not used as definitive evidence of the succession's thermal-maturity stage [47].

The data analysed in the multivariate analyses in the present study are also restricted to a small number of subjects (n = 20), and the group sizes are unequal (low = 4, middle = 11, and upper = 5). This imbalance and outliers like WX-11 (HI = 601.03 mg HC/g TOC) and WX-20 (TOC = 3.82 wt%; S1 = 4.45 mg HC/g rock; S2 = 9.12 mg HC/g rock) can affect cluster-boundary definitions and principal component loadings. Thus, separation of the lower Maastrichtian interval in PCA and clustering is recognised as geochemically indicative rather than statistically definitive, and use of the results for the broader basin should reflect this small sample size. However, the univariate ANOVA and Tukey/Games-Howell tests also corroborate the key geochemical trends, which are less prone to multivariate clustering artefacts, including an increase in TOC, S1+S2, and S3 in the lower interval.

The relationship between depth and S1+S2 is moderately positive (R^2 = 0.387), with deeper samples generally recording higher values. This trend probably reflects greater organic richness and higher remaining S2 in the Lower interval. However, S1 values in the Lower interval exceed the threshold commonly associated with possible migrated hydrocarbons, indicating that part of the S1+S2 signal may reflect migration rather than indigenous generation alone. The observed relationship should therefore be interpreted as the combined effect of source-rock richness, remaining generative potential, and possible hydrocarbon migration rather than as a simple consequence of progressive maturation and expulsion.

Although geochemical heterogeneity in Cretaceous source rocks of the Dahomey and Tano basins has been documented previously [22, 27, 45], this study provides three specific contributions. First, it presents a depth-resolved evaluation of the Maastrichtian Araromi succession within a single well, demonstrating systematic vertical variation in organic richness, kerogen characteristics, thermal maturity, and hydrocarbon-generation potential across the

DOI: https://doi.org/10.53704/fujnas.v15i2.1572

Lower, Middle, and Upper depth-defined intervals. Previous studies have generally treated the Araromi Formation more broadly, with comparatively limited emphasis on such within-formation vertical variability. Second, the observed geochemical differences are supported by complementary univariate and multivariate statistical analyses, including ANOVA, Tukey HSD/Games–Howell post-hoc tests, PCA, HCA, and K-means clustering. These analyses particularly distinguish the Lower interval, while also showing appreciable overlap and internal heterogeneity within the Middle and Upper intervals; consequently, the statistical results support vertical geochemical differentiation but do not independently validate three discrete chronostratigraphic units. Third, the elevated S1 values in the Lower interval suggest migrated hydrocarbons, highlighting the need to distinguish free migrated hydrocarbons from indigenous remaining generative potential when evaluating source-rock quality. This observation has implications for source-rock assessment and petroleum-system modelling in the eastern Dahomey Basin.

Conclusion

A Rock-Eval and TOC analysis of the Maastrichtian Araromi shales from a single well (1128–2181 m) in the eastern Dahomey Basin indicates that the Lower Maastrichtian interval has the greatest organic richness (TOC = 3.12 wt%), the highest remaining generative potential (S2 = 8.08 mg HC/g rock), and the highest source potential (S1+S2 = 12.37 mg HC/g rock), with predominantly Type II/III kerogen. Maturity, assessed using Tmax and Tmax-derived apparent %Ro, varies substantially across the studied succession, with the Lower interval recording the highest apparent maturity indicators. However, the anomalously high Tmax values and absence of directly measured vitrinite reflectance preclude definitive assignment of a post-oil-window maturity stage. The statistical analyses demonstrate significant geochemical variation through the studied depth interval, with the Lower interval showing the clearest differentiation from the overlying samples. Although a three-cluster solution provides a useful exploratory representation of this heterogeneity, silhouette analysis favours two clusters, and the Upper and Middle intervals show substantial overlap. The multivariate results therefore should not be interpreted as independent validation of three discrete chronostratigraphic units. The study's main contribution is its single-well, depth-resolved characterisation of vertical geochemical heterogeneity and its identification of possible migrated hydrocarbons in the Lower interval. But the single-well model, the use of apparent %Ro calculated from Tmax, and the lack of biomarker and basin-modelling data mean that only tentative conclusions can be drawn regarding the whole region. Further study would benefit from additional wells, direct vitrinite reflectance, biomarkers, and basin modelling.

References

1. Hunt JM. Petroleum geochemistry and geology. 2nd ed. W.H. Freeman; 1995.
2. El Atfy H, Ghassal BI, editors. Advances in petroleum source rock characterizations: integrated methods and case studies. 1st ed. Springer; 2023. https://doi.org/10.1007/978-3-031-16396-8
3. Awadh SM, Al-Mimar HS. Source rock evaluation in petroleum geology: standardized terminology and integrated geochemical criteria. Iraqi Journal of Petroleum Geology and Geophysics. 2026;16:Article 16. https://jks.kus.edu.iq/index.php/ijpgg/article/view/16
4. Tissot BP, Welte DH. Petroleum formation and occurrence. 2nd rev. ed. Springer-Verlag; 1984. https://doi.org/10.1007/978-3-642-87813-8
5. Peters KE, Cassa MR. Applied source rock geochemistry. In: Magoon LB, Dow WG, editors. The petroleum system - From source to trap. AAPG Memoir 60. American Association of Petroleum Geologists; 1994. p. 93-120. https://doi.org/10.1306/M60585C5
6. Falufosi MO, Osinowo OO. Geology and hydrocarbon potential of the Nigerian sector of Dahomey Basin. Journal of Sedimentary Environments. 2021;6:335-358. https://doi.org/10.1007/s43217-021-00062-7
7. Bolaji TA, Ndukwe OS, Oyebamiji AR, Ikegwuonu ON. Palynological age control and paleoenvironments of the Paleogene strata in Eastern Dahomey Basin, Southwestern Nigeria. Scientific Reports. 2020;10:8991. https://doi.org/10.1038/s41598-020-65462-7
8. Toyin A, Zhong N, Idris FO, Adekeye O, Shi S. Geochemical evidences linking the Lower Cretaceous source rocks to the biodegraded bitumen seeps and tar sands in the Gulf of Guinea Basin. Organic Geochemistry. 2024;197:104866. https://doi.org/10.1016/j.orggeochem.2024.104866
9. Adekeye OA, Akande SO. The principal source rocks for petroleum generation in the Dahomey Basin, southwestern Nigeria. Continental Journal of Earth Sciences. 2010;5(1):42-55. https://www.academia.edu/82106572/The_Principal_Source_Rocks_For_Petroleum_Generation_In_The_Dahomey_Basin_Southwestern_Nigeria
10. Akande SO, Adekeye OA, Adeoye JA, Jacob N, Lufadeju G. Paleoecologic and organic geochemical assessment of Cretaceous hydrocarbon source rocks in the Gulf of Guinea: new insights from eastern Dahomey and Benue Rift Basins with implications for the Cenomanian-Coniacian petroleum system. Search and Discovery Article. 2012;50722:1-10. https://www.semanticscholar.org/paper/Paleoecologic-and-Organic-Geochemical-Assessment-of-Akande-Adekeye/625d5f09025b436ac2980ead8f60754dbfac64dd
11. Billman HG. Offshore stratigraphy and paleontology of the Dahomey embayment, West Africa. Géologie Méditerranéenne. 1984;11(1-2):132. https://www.persee.fr/doc/geolm_0397-2844_1984_num_11_1_1299
12. Okunubi MO. Structure and sediment thickness mapping of eastern Dahomey (Benin) Basin, southwest Nigeria [doctoral dissertation]. Obafemi Awolowo University; 2022. https://ir.oauife.edu.ng/handle/123456789/6855
13. Adeigbe O, Oyekola C. Geology and geochemistry of sediments from Lewumeji and Idogun wells, Eastern Dahomey Basin Southwestern Nigeria. Journal of Environment and Earth Science. 2020;10(5). https://doi.org/10.7176/JEES/10-5-03

DOI: https://doi.org/10.53704/fujnas.v15i2.1572

14. Okosun EA. A review of the Cretaceous stratigraphy of the Dahomey Embayment, West Africa. Cretaceous Research. 1990;11(1):17-27. https://doi.org/10.1016/S0195-6671(05)80040-0
15. Ogundipe O, Adekeye O, Akande S, Adeyilola A. Biostratigraphic studies and source rock evaluation of Araromi Formation, Eastern Dahomey Basin, Southwestern Nigeria [conference presentation]. AAPG Annual Convention and Exhibition 2020; Online/Virtual; 2020. https://www.searchanddiscovery.com/pdfz/abstracts/pdf/2022/91200ace/abstracts/ndx_ogundipe.pdf.html
16. Gebhardt H, Adekeye OA, Akande SO. Late Paleocene to Initial Eocene Thermal Maximum (IETM) foraminiferal biostratigraphy and paleoecology of the Dahomey Basin, Southwestern Nigeria. Jahrbuch der Geologischen Bundesanstalt. 2011;3:407-419. https://www.researchgate.net/profile/Holger-Gebhardt/publication/285116713_Late_Paleocene_to_Initial_Eocene_Thermal_Maximum_IETM_foraminiferal_biostratigraphy_and_paleoecology_of_the_Dahomey_Basin_southern_Nigeria/links/59c8deaf458515548f3d9686/Late-Paleocene-to-Initial-Eocene-Thermal-Maximum-IETM-foraminiferal-biostratigraphy-and-paleoecology-of-the-Dahomey-Basin-southern-Nigeria.pdf
17. Adekeye OA, Akande SO, Adeoye JA. The assessment of potential source rocks of Maastrichtian Araromi formation in Araromi and Gbekebo wells Dahomey Basin, southwestern Nigeria. Heliyon. 2019;5(5):e01561. https://doi.org/10.1016/j.heliyon.2019.e01561
18. Adeoye JA, Akande SO, Adekeye OA, Sonibare WA, Ondrak R, Dominik W, et al. Source rock maturity and petroleum generation in the Dahomey Basin SW Nigeria: insights from geologic and geochemical modelling. Journal of Petroleum Science and Engineering. 2020;195:107844. https://doi.org/10.1016/j.petrol.2020.107844
19. Ola-Buraimo OA, Oluwajana OA, Olaniyan A, Omoboriowo AO. Palynological investigation of a type section of early Maastrichtian Arimogija-Okeluse shale sequence, Dahomey (Benin) Embayment, southwestern Nigeria. International Journal of Science and Emerging Technologies. 2012;3(1):37-45. https://www.researchgate.net/publication/279179964_Palynological_Investigation_of_a_Type_Section_of_Early_Maastrichtian_Arimogija_-_Okeluse_Shale_Sequence_Dahomey_Benin_Embayment_Southwestern_Nigeria
20. Adamolekun OJ, Busch B, Suess MP, Molenaar N, Hilgers C. Petrography and reservoir quality controls in shallow transitional marine Cretaceous-Paleogene deposits in the Dahomey Basin, Nigeria. Journal of African Earth Sciences. 2022;186:104437. https://doi.org/10.1016/j.jafrearsci.2021.104437
21. Ikhane PR, Omosanya KO, Akinmosin AA, Odugbesan AB. Electrical resistivity imaging (ERI) of slope deposits and structures in some parts of Eastern Dahomey Basin. Journal of Applied Sciences. 2012;12(8):716-726. https://doi.org/10.3923/jas.2012.716.726
22. Oluwajana OA, Opatola AO, Adamolekun OJ, Ndukwe OS, Olawuyi GT, Ofiwe CU, et al. Sedimentation, depositional environments, and hydrocarbon potential of the Maastrichtian-Paleocene Araromi Formation, eastern Dahomey (Benin) Basin, southwestern Nigeria. Journal of Petroleum Exploration and Production Technology. 2021;11:3917-3934. https://doi.org/10.1007/s13202-021-01262-7
23. Mohammed S, Opuwari M, Titinchi S. Source rock evaluation of Afowo clay type from the Eastern Dahomey Basin, Nigeria: insights from different measurements. Scientific Reports. 2020;10:12036. https://doi.org/10.1038/s41598-020-68918-y
24. Alege TS, Tella T, Aigbadon GO. Lithofacies, bio-sequence stratigraphy and paleoenvironment of the Cretaceous-Neogene at the BG-1 well, offshore Eastern Dahomey Basin, Nigeria: implications for future exploration and development efforts. Carbonates and Evaporites. 2024;39(2). https://doi.org/10.1007/s13146-024-00953-6
25. Adebambo B, Oluwajana OA, Adebisi AA. Paleobiogeographic affinities and paleoecological significance of Paleogene ostracods from Eastern Benin Basin, Southwestern Nigeria. Ife Journal of Science. 2023;25(1):27-34. https://doi.org/10.4314/ijs.v25i1.4
26. Oluwajana OA, Adebambo B, Olawuyi GT, Adedokun TA, Opatola AO, Adamolekun OJ, et al. Paleoecologic implications of foraminiferal assemblages in the Upper Cretaceous-Paleogene strata, eastern Dahomey (Benin) Basin, southwestern Nigeria. Arabian Journal of Geosciences. 2021;14(9):1-16. https://doi.org/10.1007/s12517-021-07038-x
27. Aigbadon GO, Overare B, Akakuru OC, Obasi AI, Ocheli A, Akudo EO, et al. Evolution of petroleum systems and hydrocarbon migration in the Dahomey Basin: insights from basin modeling, machine learning and geochemical analysis. Solid Earth Sciences. 2025;10:100273. https://doi.org/10.1016/j.sesci.2025.100273
28. Omatsola ME, Adegoke OS. Tectonic evolution and Cretaceous stratigraphy of the Dahomey Basin. Journal of Mining and Geology. 1981;18:130-137.
29. Adekeye OA. Aspects of sedimentology, geochemistry and hydrocarbon potentials of Cretaceous-Tertiary sediments in the Dahomey Basin, south-western Nigeria [doctoral dissertation]. University of Ilorin; 2005. 202 p.
30. Espitalié J, Laporte JL, Madec M, Marquis F, Leplat P, Paulet J, et al. Méthode rapide de caractérisation des roches mères, de leur potentiel pétrolier et de leur degré d'évolution. Revue de l'Institut Français du Pétrole. 1977;32(1):23-42. https://doi.org/10.2516/ogst:1977002
31. Jarvie DM, Claxton BL, Henk F, Breyer JT. Oil and shale gas from the Barnett Shale, Ft. Worth Basin, Texas. AAPG Bulletin. 2001;85(13):1-27. https://doi.org/10.1306/8626E28D-173B-11D7-8645000102C1865D
32. Peters KE, Walters CC, Moldowan JM. The biomarker guide. Vol. 2, Biomarkers and isotopes in petroleum exploration and earth history. 2nd ed. Cambridge University Press; 2005. https://doi.org/10.1017/CBO9781107326040
33. Jolliffe IT, Cadima J. Principal component analysis: a review and recent developments. Philosophical Transactions of the Royal Society A: Mathematical, Physical and Engineering Sciences. 2016;374(2065):20150202. https://doi.org/10.1098/rsta.2015.0202
34. Ward JH Jr. Hierarchical grouping to optimize an objective function. Journal of the American Statistical Association. 1963;58(301):236-244. https://doi.org/10.1080/01621459.1963.10500845
35. Tukey JW. Comparing individual means in the analysis of variance. Biometrics. 1949;5(2):99-114. https://doi.org/10.2307/3001913
36. Abubakar R, Adomako-Ansah K, Marfo SA, Fenyi C, Owusu JA. Integrated geochemical and statistical evaluation of the source rock potential in the deep-water, Western Basin of Ghana. Journal of Petroleum Science and Engineering. 2022;220(2):111164. https://doi.org/10.1016/j.petrol.2022.111164
37. Saadu MB, Jimoh AY, Adekeye OA, Issa TA. Biostratigraphy and palaeoecological studies of the Late Cretaceous-Tertiary sediments in the Dahomey Basin, Nigeria. European Journal of Environment and Earth Sciences. 2022;3(4):41-47. https://doi.org/10.24018/ejgeo.2022.3.4.274
38. Johnson TD, Oluwajana OA, Omietimi EJ, Ayo-Bali AE, Odondiri OD, Igili CO, et al. Elemental geochemistry of Cretaceous deposits in the Dahomey Basin (Nigeria): implications for paleoclimatic and paleoenvironmental reconstructions. Journal of African Earth Sciences. 2024;216:105311. https://doi.org/10.1016/j.jafrearsci.2024.105311
39. Tyson RV. Sedimentary organic matter: organic facies and palynofacies. Chapman & Hall; 1995. https://doi.org/10.1007/978-94-011-0739-6
40. Toyin A, Idris FO, Konan NFDS, Adekeye O, Ayok J. Characteristics of Cretaceous outcrop shales and coals from the Nigeria Frontier Basins as hydrocarbon source rocks: insights from open system pyrolysis. Journal of the Geological Society of India. 2025;101(11):1652-1662. https://doi.org/10.17491/jgsi/2025/174289
41. Abubakar U, Hohl SV, Usman MB, Maigari AS, Tchouatcha MS, Tabale RP, et al. Provenance history, depositional conditions and tectonic settings during late Cenomanian-early Turonian time in the Gongola Sub-Basin of the Upper Benue Trough Nigeria: evidence from major and trace elements geochemistry of the Kanawa shales from the Pindiga Formation. Journal of African Earth Sciences. 2024;211:105168. https://doi.org/10.1016/j.jafrearsci.2024.105168
42. Martins OE, Mosto OK, Ifeanyi OA. Aeromagnetic interpretation of basement structure and architecture of the Dahomey Basin, Southwestern Nigeria. NRIAG Journal of Astronomy and Geophysics. 2021;10(1):93-109. https://doi.org/10.1080/20909977.2021.1880817

DOI: https://doi.org/10.53704/fujnas.v15i2.1572

43. Ekweozor CM, Nwachukwu JI. The origin of tar sands of southwestern Nigeria. Nigerian Association of Petroleum Explorationists Bulletin. 1989;4(2):82-84.
44. Bolaji TA, Victor-Oji CO, Adedeji OA. Geochemical characterisation of the Turonian-Maastrichtian bituminous sands in Dahomey Basin, Southwestern Nigeria. Energy Exploration & Exploitation. 2023;41(3):922-940. https://doi.org/10.1177/01445987231159936
45. Amoako K, Zhong N, Shi S, Konan NFDS, Osei-Boakye NP, Foli G, et al. Organic geochemical heterogeneity of Cretaceous mudrocks and reassessment of oil sources in the Tano Basin, Ghana. Marine and Petroleum Geology. 2024;162:106697. https://doi.org/10.1016/j.marpetgeo.2024.106697
46. Toyin A, Idris FO, Adekeye O, Ayok J, Konan NFDS. Organic geochemistry and hydrocarbon generation characteristics of Cretaceous outcrop source rocks from the Nigerian Frontier Basins. Journal of African Earth Sciences. 2025;231:105766. https://doi.org/10.1016/j.jafrearsci.2025.105766
47. Yang S, Horsfield B. Critical review of the uncertainty of Tmax in revealing the thermal maturity of organic matter in sedimentary rocks. Int J Coal Geol. 2020;225:103500. https://doi.org/10.1016/j.coal.2020.103500

==========
APPENDIX: STATISTICAL ANALYSIS OUTPUTS
Dahomey Basin Maastrichtian Shales
==========

==========
TABLE A1: LEVENE'S TEST FOR HOMOGENEITY OF VARIANCE
==========
TOC : Levene's p = 0.9175 -> Met
S1 : Levene's p = 0.1274 -> Met
S2 : Levene's p = 0.1898 -> Met
S3 : Levene's p = 0.7202 -> Met
Tmax : Levene's p = 0.6239 -> Met
HI : Levene's p = 0.0501 -> Met
OI : Levene's p = 0.2777 -> Met
S2_S3 : Levene's p = 0.1008 -> Met
PI : Levene's p = 0.2131 -> Met
S1_S2 : Levene's p = 0.0360 -> Violated
Ro_calc : Levene's p = 0.6235 -> Met

==========
TABLE A2: ANOVA WITH EFFECT SIZES
==========
TOC : F = 20.0515, p = 0.000034, Test = One-way ANOVA
S1 : F = 55.1133, p = 0.000000, Test = One-way ANOVA
S2 : F = 16.8329, p = 0.000093, Test = One-way ANOVA
S3 : F = 93.7108, p = 0.000000, Test = One-way ANOVA
Tmax : F = 1.1182, p = 0.349745, Test = One-way ANOVA
HI : F = 2.4244, p = 0.118491, Test = One-way ANOVA
OI : F = 14.8640, p = 0.000185, Test = One-way ANOVA
S2_S3 : F = 6.5708, p = 0.007689, Test = One-way ANOVA
PI : F = 11.1914, p = 0.000792, Test = One-way ANOVA
S1_S2 : F = 63.7986, p = 0.000007, Test = Welch's ANOVA
Ro_calc : F = 1.1180, p = 0.349810, Test = One-way ANOVA

==========
TABLE A3: TUKEY HSD POST-HOC
==========

Parameter	Comparison	Mean_Diff	Standard_Error	T_value	p_value	Significant
TOC	Lower vs Middle	1.7289	0.2791	6.1940	0.0000	Yes
TOC	Lower vs Upper	0.9425	0.3207	2.9391	0.0236	Yes
TOC	Middle vs Upper	-0.7864	0.2578	-3.0498	0.0188	Yes
S1	Lower vs Middle	2.4914	0.2550	9.7683	0.0000	Yes
S1	Lower vs Upper	2.6950	0.2930	9.1971	0.0000	Yes
S1	Middle vs Upper	0.2036	0.2356	0.8643	0.6693	No
S2	Lower vs Middle	3.5455	0.6145	5.7700	0.0001	Yes
S2	Lower vs Upper	2.9320	0.7060	4.1532	0.0018	Yes
S2	Middle vs Upper	-0.6135	0.5676	-1.0807	0.5384	No
S3	Lower vs Middle	1.5680	0.1154	13.5877	0.0000	Yes
S3	Lower vs Upper	1.3205	0.1326	9.9601	0.0000	Yes
S3	Middle vs Upper	-0.2475	0.1066	-2.3214	0.0798	No
OI	Lower vs Middle	30.8084	6.0406	5.1002	0.0002	Yes
OI	Lower vs Upper	32.8915	6.9402	4.7393	0.0005	Yes
OI	Middle vs Upper	2.0831	5.5801	0.3733	0.9264	No
S2_S3	Lower vs Middle	-5.9623	1.7008	-3.5055	0.0072	Yes

DOI: https://doi.org/10.53704/fujnas.v15i2.1572

S2_S3	Lower vs Upper	-2.9830	1.9541	-1.5265	0.3038	No
S2_S3	Middle vs Upper	2.9793	1.5712	1.8962	0.1701	No
PI	Lower vs Middle	0.0648	0.0205	3.1554	0.0151	Yes
PI	Lower vs Upper	0.1115	0.0236	4.7277	0.0005	Yes
PI	Middle vs Upper	0.0467	0.0190	2.4642	0.0608	No

TABLE A4: GAMES-HOWELL POST-HOC FOR S1+S2

Parameter	Comparison	Mean_Diff	Standard_Error	T_value	df	p_value	Significant
S1+S2	Lower vs Middle	6.0368	0.6485	9.3083	10.3102	0.0000	Yes
S1+S2	Lower vs Upper	5.6270	0.5029	11.1900	4.9979	0.0002	Yes
S1+S2	Middle vs Upper	-0.4098	0.5462	-0.7503	13.7001	0.7385	No

TABLE A5: PEARSON CORRELATION MATRIX

	TOC	S1	S2	S3	Tmax	HI	OI	S2_S3	PI	S1_S2	Ro_calc
TOC	1.000	0.665	0.767	0.879	0.180	-0.620	0.453	-0.738	0.207	0.758	0.179
S1	0.665	1.000	0.828	0.871	0.441	-0.063	0.758	-0.440	0.763	0.935	0.441
S2	0.767	0.828	1.000	0.855	0.371	-0.031	0.695	-0.475	0.295	0.973	0.371
S3	0.879	0.871	0.855	1.000	0.329	-0.330	0.793	-0.731	0.460	0.899	0.329
Tmax	0.180	0.441	0.371	0.329	1.000	0.159	0.372	-0.148	0.313	0.416	1.000
HI	-0.620	-0.063	-0.031	-0.330	0.159	1.000	0.140	0.608	0.021	-0.045	0.160
OI	0.453	0.758	0.695	0.793	0.372	0.140	1.000	-0.612	0.446	0.752	0.372
S2_S3	-0.738	-0.440	-0.475	-0.731	-0.148	0.608	-0.612	1.000	-0.079	-0.481	-0.147
PI	0.207	0.763	0.295	0.460	0.313	0.021	0.446	-0.079	1.000	0.502	0.314
S1_S2	0.758	0.935	0.973	0.899	0.416	-0.045	0.752	-0.481	0.502	1.000	0.416
Ro_calc	0.179	0.441	0.371	0.329	1.000	0.160	0.372	-0.147	0.314	0.416	1.000

TABLE A6: PCA EXPLAINED VARIANCE

PC	Eigenvalue	Individual_Variance_%	Cumulative_Variance_%
PC1	5.0852	53.68	53.68
PC2	2.0250	21.38	75.05
PC3	1.1420	12.05	87.11
PC4	0.8464	8.93	96.04
PC5	0.3198	3.38	99.42
PC6	0.0385	0.41	99.82
PC7	0.0112	0.12	99.94
PC8	0.0056	0.06	100.00
PC9	0.0000	0.00	100.00

TABLE A7: PCA LOADINGS

	PC1	PC2	PC3
TOC	0.3459	-0.4108	-0.2511
S1	0.4318	-0.0091	0.2217
S2	0.3971	-0.0964	0.0714
S3	0.4261	-0.2203	0.0275
HI	-0.0660	0.5372	0.5039
OI	0.3675	0.0612	0.3282
Tmax	0.2656	0.4816	-0.4421
PI	0.2723	0.1292	0.3607
Ro_calc	0.2655	0.4821	-0.4413

TABLE A8: PCA SCORES

Sample_ID	Age	Depth	PC1	PC2	PC3
WX-01	Upper	1128	-0.7664	-2.4091	-0.7240
WX-02	Upper	1158	-1.4962	-1.8855	-0.4165
WX-03	Upper	1191	-1.4027	-1.2526	0.3269
WX-04	Upper	1224	-0.0952	1.1595	-1.8128
WX-05	Upper	1254	-0.0517	1.0819	-2.0803
WX-06	Middle	1287	-0.6323	0.2278	-1.4662
WX-07	Middle	1323	-0.6217	-1.0245	0.5868
WX-08	Middle	1353	0.4868	1.9764	-0.8149
WX-09	Middle	1389	-1.8428	-1.5110	0.5413

DOI: https://doi.org/10.53704/fujnas.v15i2.1572

WX-10	Middle	1419	-0.4899	0.0823	0.2351
WX-11	Middle	1578	-0.2910	2.2355	1.8521
WX-12	Middle	1608	-2.4588	1.0352	1.2168
WX-13	Middle	1665	-1.3679	1.6725	0.3124
WX-14	Middle	1695	-1.9949	-0.8283	0.9943
WX-15	Middle	1728	-2.4928	-0.8412	-0.2717
WX-16	Middle	1980	-0.7660	2.1930	-0.0892
WX-17	Lower	2028	4.3670	-0.1768	0.1441
WX-18	Lower	2100	5.0156	-0.6529	-0.6918
WX-19	Lower	2133	3.0411	-1.4419	0.4204
WX-20	Lower	2181	3.8598	0.3598	1.7372

==========

TABLE A9: COPHENETIC CORRELATION COEFFICIENT

==========

Cophenetic Correlation Coefficient: 0.8743

Interpretation: Good - dendrogram faithfully represents pairwise distances

Table A9 saved:

Metric	Value	Linkage_Method	Distance_Metric	Interpretation
Cophenetic Correlation Coefficient	0.8743	Ward	Squared Euclidean	Good - dendrogram faithfully represents pairwise distances

==========

TABLE A10: HCA CLUSTER ASSIGNMENTS

==========

Sample_ID	Age	Depth	HCA_Cluster
WX-01	Upper	1128	2
WX-02	Upper	1158	2
WX-03	Upper	1191	2
WX-04	Upper	1224	3
WX-05	Upper	1254	3
WX-06	Middle	1287	3
WX-07	Middle	1323	2
WX-08	Middle	1353	3
WX-09	Middle	1389	2
WX-10	Middle	1419	3
WX-11	Middle	1578	3
WX-12	Middle	1608	3
WX-13	Middle	1665	3
WX-14	Middle	1695	2
WX-15	Middle	1728	2
WX-16	Middle	1980	3
WX-17	Lower	2028	1
WX-18	Lower	2100	1
WX-19	Lower	2133	1
WX-20	Lower	2181	1

==========

TABLE A11: SILHOUETTE SCORES FOR K-MEANS

==========

k = 2: Silhouette Score = 0.4638

k = 3: Silhouette Score = 0.3646

k = 4: Silhouette Score = 0.3588

k = 5: Silhouette Score = 0.2677

k = 6: Silhouette Score = 0.2345

==========

TABLE A12: K-MEANS CLUSTER CENTERS (k=3, raw units)

==========

	TOC	S1	S2	S3	HI	OI	Tmax	PI	Ro_calc
Cluster 0	1.4557	1.7943	4.9571	0.5900	371.7257	42.3186	577.1429	0.2643	3.2300
Cluster 1	1.7822	1.6800	4.5467	0.5933	272.2989	32.3089	455.2222	0.2711	1.0322
Cluster 2	3.1225	4.2850	8.0800	2.0825	265.7925	68.1475	564.2500	0.3475	2.9975

==========

TABLE A13: K-MEANS CLUSTER MEMBERSHIP (k=3)

==========

Sample_ID	Age	Depth	KMeans_Cluster
WX-01	Upper	1128	1
WX-02	Upper	1158	1

DOI: https://doi.org/10.53704/fujnas.v15i2.1572

WX-03	Upper	1191	1
WX-04	Upper	1224	0
WX-05	Upper	1254	0
WX-06	Middle	1287	0
WX-07	Middle	1323	1
WX-08	Middle	1353	0
WX-09	Middle	1389	1
WX-10	Middle	1419	1
WX-11	Middle	1578	0
WX-12	Middle	1608	1
WX-13	Middle	1665	0
WX-14	Middle	1695	1
WX-15	Middle	1728	1
WX-16	Middle	1980	0
WX-17	Lower	2028	2
WX-18	Lower	2100	2
WX-19	Lower	2133	2
WX-20	Lower	2181	2

==========

TABLE A14: SUMMARY STATISTICS BY INTERVAL

==========

	TOC		S1		S2		S3		Tmax		HI		OI		S2_S3		PI		S1_S2		Ro_calc	
	mean	std	mean	std	mean	std	mean	std	mean	std	mean	std	mean	std	mean	std	mean	std	mean	std	mean	std
Age																						
Lower	3.1225	0.6541	4.2850	0.4937	8.0800	1.1273	2.0825	0.2566	564.25	41.8599	265.7925	56.2897	68.1475	10.9227	3.8950	0.4968	0.3475	0.0532	12.3650	0.8662	2.9975	0.7518
Middle	1.3936	0.4094	1.7936	0.4963	4.5345	1.1755	0.5145	0.1957	507.00	62.5460	349.6673	124.6706	37.3391	11.8877	9.8573	3.7264	0.2827	0.0329	6.3282	1.6010	1.9664	1.1257
Upper	2.1800	0.4810	1.5900	0.1114	5.1480	0.5471	0.7620	0.1446	512.00	89.0337	241.2860	34.2446	35.2560	3.4819	6.8780	1.0782	0.2360	0.0207	6.7380	0.5714	2.0540	1.6081

DOI: https://doi.org/10.53704/fujnas.v15i2.1572